ISSN 1075-7015, Geology of Ore Deposits, 2006, Vol. 48, No. 3, pp. 193–214. © Pleiades Publishing, Inc., 2006.
Original Russian Text © A.I. Brusnitsyn, 2006, published in Geologiya Rudnykh Mestorozhdenii, 2006, Vol. 48, No. 3, pp. 225–248.

Mineralogy and Metamorphism Conditions of Manganese Ore at the South Faizulino Deposit, the Southern Urals, Russia

A. I. Brusnitsyn

St. Petersburg State University, Universitetskaya nab. 7/9, St. Petersburg, 199034 Russia

Received June 16, 2005

Abstract—The mineralogy of slightly metamorphosed manganese ore at the South Faizulino hydrothermal–sedimentary deposit in the southern Urals has been studied; 32 minerals were identified. Quartz, hausmannite, rhodochrosite, tephroite, ribbeite, pyroxmangite, and caryopilite are major minerals; calcite, kutnahorite, alleghanyite, spessartine, rhodonite, clinochlore, and parsettensite are second in abundance. This mineralic composition was formed in the process of gradual burial of ore beneath the sequence of Middle Devonian–Lower Carboniferous rocks. The highest parameters of metamorphism are $T \approx 250$°C and $P \approx 2.5$ kbar. The relationships between minerals and their assemblages made it possible to reconstruct the succession of ore transformation with gradually increasing temperature and pressure. Manganese accumulated in the initial sediments as oxides and a gel-like Mn–Si phase. Rhodochrosite and neotocite were formed at the diagenetic stage. In the course of a further increase in temperature and pressure, neotocite was replaced with caryopilite; ribbeite, tephroite, pyroxmangite, and other silicates crystallized afterwards. In addition to the *PT* parameters, the formation of various metamorphic mineral assemblages was controlled by the Mn/(Mn + Si) ratio in ore and X_{CO_2} in pore solution. The latter parameter was determined by the occurrence of organic matter in the ore-bearing rocks. Ore veinlets as products of local hydrothermal redistribution of Mn, Si, and CO_2 were formed during tectonic deformations in the Middle Carboniferous and Permian.

DOI: 10.1134/S1075701506030032

INTRODUCTION

The South Faizulino deposit, which is situated in the southern Urals 20 km southeast of the town of Sibai, is one of the largest among the numerous hydrothermal–sedimentary manganese deposits known in the region (Kontar et al., 1999; Mikhailov, 2001). The grade of metamorphism of ore-bearing rocks at the deposit is not higher than the conditions of prehnite–pumpellyite facies (*Copper…*, 1985; Rusinov et al., 1992). Therefore, the mineralogy of manganese ore is very specific here: clearly expressed newly formed metamorphic minerals are combined with relics of typical sedimentary mineral assemblages. The study of such an ore allows characterization of rare manganese minerals, on the one hand, and gives a good opportunity to trace the transformation of the phase composition of Mn-bearing sediments as a result of a gradual increase in temperature and pressure, on the other hand. Mineralogical information is necessary for estimation of the economic outlook for this deposit.

The available information on the mineralogy of the South Faizulino deposit have so far remained extremely scanty (Gavrilov, 1972; Kalinin, 1978). The objective of my study was to fill this gap. Works were carried out in 1997–2003 that focused on oxide–carbonate–silicate ore of the main southern lode, which is currently mined. The results obtained are discussed in this paper. An attempt is made to reconstruct the transformation of Mn-bearing rocks affected by increasing temperature and pressure on the basis of comparison of the data obtained with data on other, genetically allied deposits, together with physicochemical analysis of phase equilibria.

Corresponding author A.I. Brusnitsyn. E-mail: brusspb@yandex.ru

BRIEF CHARACTERISTICS OF THE DEPOSIT

The South Faizulino lode is a typical example of stratiform manganese deposits hosted in cherty units of volcanic zones. The geology, petrography, and stages of ore deposition were considered in detail previously (Brusnitsyn and Zhukov, 2005).

The deposit is located at the western margin of the Magnitogorsk paleovolcanic belt (Fig. 1a). The area is composed of Devonian volcanic and volcanosedimentary complexes formed in the West Magnitogorsk ensimatic island arc and the Sibai interarc basin, which adjoins it in the east (e.g., Zaikov, 1991; Seravkin et al., 1992). The Mn-bearing rocks are localized in the sedimentary fill of the interarc basin thrust over island-arc volcanics. The Emsian–Eifelian Irendyk Formation of basaltic andesites, the Eifelian Bugulygyr cherty unit, and the Givetian–Lower Frasnian Ulutau Formation of tephroterrigenous rocks are known at the deposit.

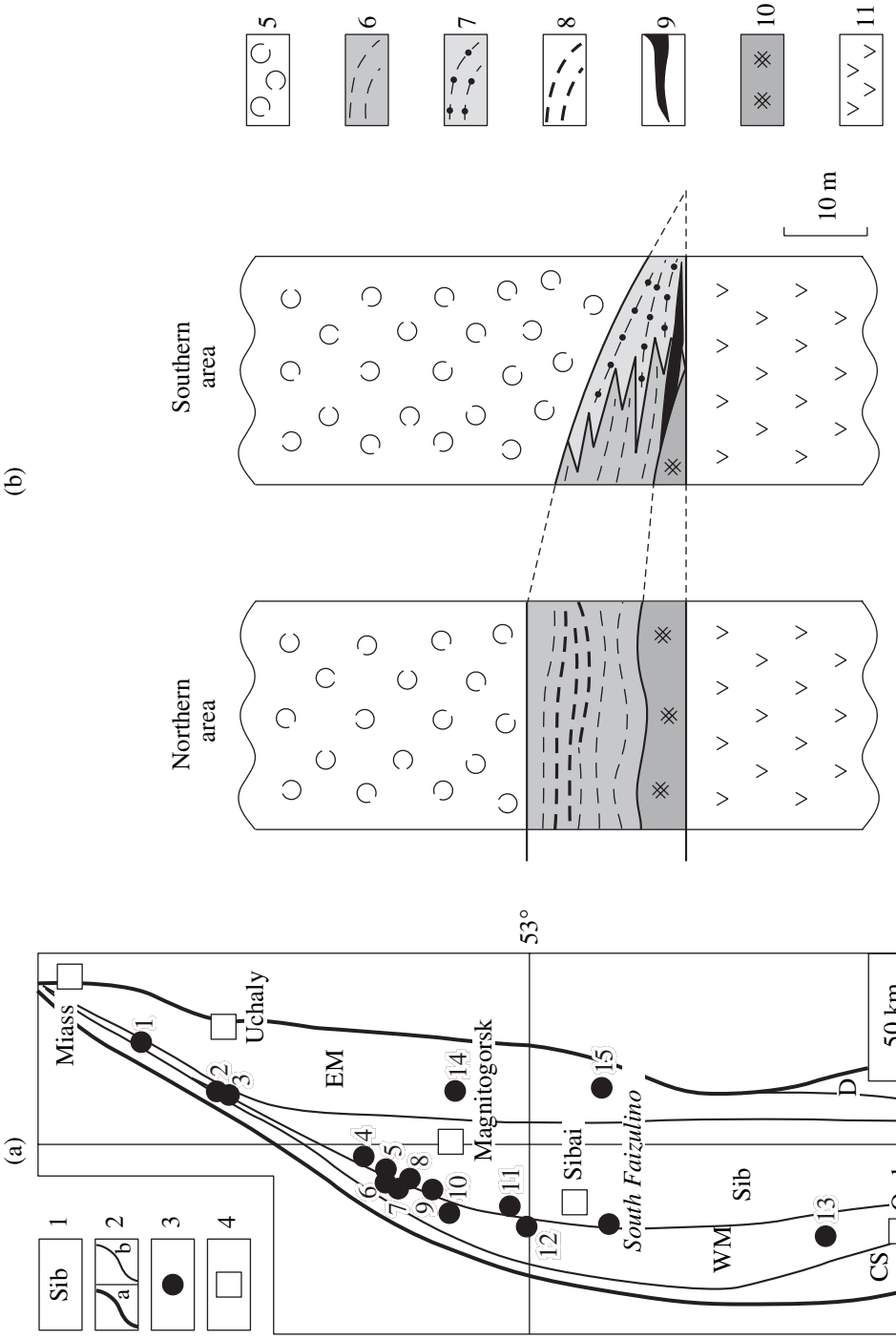

Fig. 1. (a) Location of major manganese deposits in the Magnitogorsk paleovolcanic belt after Zaikov (1991) and (b) schematic stratigraphic columns of the South Faizulino deposit after Brusnitsyn and Zhukov (2005). (1) Paleogeodynamic zone; (2) boundaries of (a) Magnitogorsk paleovolcanic belt and (b) other paleogeodynamic zones; (3) manganese deposit; (4) town; (5–11) volcanic, volcanosedimentary, and hydrothermal–sedimentary rocks: (5) Givetian–Frasnian Ulutau Formation: rhythmic intercalation of volcanomictic sandstone and cherty siltstone and mudstone; (6–10) Eifelian Bugulygyr Unit: (6) sealing-wax-red jasper, (7) gray cherty siltstone, (8) braunite interlayers in jasper, (9) oxide–carbonate–silicate manganese ore, (10) jasperite; (11) Emsian–Eifelian Irendyk Formation: basalt and basaltic andesite (lava, lava breccia, and hyaloclastite). Paleogeodynamic zones (letters in Fig. 1a): (CS) Cis-Sakmara, a an accretionary prism fragment; (WM) West Magnitogorsk island arc; (Sib) Sibai interarc basin; (EM) East Magnitogorsk island arc; (D) Dombarovka backarc basin. Manganese deposits (numerals in Fig. 1a): (1) Kozhaevo, (2) Tetrauk, (3) Urazovo, (4) Gabdimovo, (5) Ayusazovo, (6) Niyazgulovo, (7) Bikkulovo, (8) Kusimovo, (9) Yalimbetovo, (10) Kyzyltash, (11) Mamilino, (12) Gubaidulino, (13) Repino–Krutorozhino, (14) Bakhtino, (15) Lis'i Gory.

Siliceous rocks of the Bugulygyr Unit bear the ore. The sequence of their deposition reflects spatiotemporal variations in sedimentation conditions of cherty and syngenetic Mn-bearing materials (Fig. 1b). The base of the section is marked by a chain of small (2–4 m thick) lenticular bodies of jasperite—a dark red hematite–quartz rock of spotty or brecciated appearance, which is considered to be a lithified counterpart of the hydrothermal ferruginous–siliceous deposits on the bottom of the present-day oceans (Zaikova and Zaikov, 2003). Upsection, they give way to the thin-banded sealing-wax-red jasper that makes up the main body of the cherty unit. At the pinch-out of this unit, the red jasper is gradually replaced in the lateral and vertical directions with thin-banded gray cherty siltstone. The total thickness of the Bugulygyr Unit in the vicinity of the deposit reaches 15–20 m.

Manganese mineralization was established in the southern and northern areas of the deposit. The southern area is the most promising. The Mn ore here is closely associated with jasperite. The flattened lenticular stratiform orebody extends for 220 m along the strike and is traced for more than 150 m down the dip, reaching 3 m in thickness. The northern flank of the manganese ore layer directly overlaps jasperite and is, in turn, overlain by the sealing-wax-red jasper. The red cherty beds pinch out southward at a short distance, and the orebody extends farther hosted in cherty siltstone. The northern area is much smaller in size. This is a small (as thick as 0.5 m) fragment of the monotonous jasper member that contains thin (up to 1.5 cm) lenses and interbeds of braunite.[1] The ore layers and the host cherty rocks in both areas, as well as the overlying tephroterrigenous sequence of the Ulutau Formation, were deformed during the Carboniferous–Permian collision and partly eroded.

Near the surface, the ore layer is replaced with supergene Mn hydroxides. At a depth of >25 m, this layer consists of slightly oxidized oxide–carbonate–silicate ore. This is fine-grained rock of heterogeneous structure and composition. The typically sedimentary and diagenetic structures and textures (banded, lenticular–bedded, pelitic, globular, colloform, spherulitic, relict organogenic, etc.) are predominant. At the same time, obvious indications of metamorphism are observed in the ore, including mosaic, granoblastic, and sheaflike structures and abundant manganese silicates (pyroxmangite, rhodonite, tephroite, ribbeite, alleghanyite, spessartine, and some other minerals) in the main ore layer.

The geological setting of the ore district indicates that the cherty rocks and volcanics, along with syngenetic manganese layers, underwent burial metamorphism (Dobretsov, 1995) under a gradually increasing loading of younger rocks accompanied by an increase in temperature and pressure. The thickness of sediments accumulated during the period between the formation of the Middle Devonian Bugulygyr Unit and the onset of active folding in the Middle Carboniferous amounts to ~8 km (Seravkin et al., 1992). At an average density of rocks of 2.8 g/cm^3 and a geothermal gradient of 30°C/km, a pressure of 2.0–2.5 kbar and a temperature of about 250°C were reached at the base of the sequence, and these values characterize the *PT* conditions of maximum sagging of manganese ore. These approximate estimates are consistent with parameters of metamorphism of volcanosedimentary rocks in this region, which correspond to the prehnite–pumpellyite facies (*Copper…*, 1985). According to Liou et al. (1985), this facies is characterized by T = 150–320°C and P = 1–4 kbar.

The local hydrothermal metasomatic processes in ore developed in close relation to tectonic deformation are recorded in stringer–reticulate and taxitic structures, where the rock is cut by numerous pyroxmangite, rhodochrosite, quartz, and other segregation or metasomatic veinlets.

On the basis of the aforesaid, four consecutive stages are recognized in the formation history of the South Faizulino deposit: (1) Middle Devonian: sedimentation and diagenesis of ore-bearing material sourced from submarine hydrothermal solutions; (2) Middle Devonian–Early Carboniferous: burial and metamorphism of Mn-bearing sediments; (3) Middle Carboniferous–Permian: formation of hydrothermal metasomatic veinlets related to the tectonic deformation of the volcanosedimentary sequence; and (4) Mesozoic–Quaternary: supergene alteration and partial denudation.

The processes that proceeded at the first stage were considered in detail previously (Brusnitsyn and Zhukov, 2005). In this paper, I focus on the mechanism and physicochemical conditions of mineral formation at the second and third stages.

MINERALIC VARIETIES OF ORE

Thirty-two minerals have been identified in the main ore layer and in the late veinlets (Fig. 2).

The main body of ore is characterized by a wide variation of mineralic composition. According to the qualitative set and quantitative proportions of minerals, five ore varieties are recognized[2]: (*a*) rhodochrosite–tephroite–ribbeite–hausmannite, (*b*) caryopilite–ribbeite–rhodochrosite–tephroite, (*c*) rhodochrosite–pyroxmangite, (*d*) rhodochrosite–pyroxmangite–quartz, and (*e*) pyroxmangite–caryopilite–quartz. Rhodochrosite–quartz and almost monomineral rhodochrosite, pyroxmangite, and rhodonite aggregates are less abundant. The rhodochrosite–pyroxmangite and rhodochrosite–pyroxmangite–quartz varieties *c* and *d* are most widespread.

[1] The braunite ore is not considered in this paper because of its limited abundance.

[2] In names of ore varieties, minerals are listed in order of increasing abundance.

No.	Mineral	Ore variety					
		main ore layer					vein complex
		a	*b*	*c*	*d*	*e*	*f*
1	Sphalerite		×	×		×	
2	Galena		×	×			
3	Alabandine		×				
4	Molybdenite	×					
5	Chalcopyrite		×	×	×	×	
6	Pentlandite		×				
7	Pyrite		×	×	×		
8	Arsenopyrite				×	×	×
9	Gersdorffite	×	×				
10	Quartz	×[1]	×[1]	●	■	■	■
11	Hematite			×		×	
12	Pyrophanite			×	×	×	
13	Hausmannite	■	×				
14	Calcite*		×	×	●	×	●
15	Rhodochrosite	■	■	■	■	●	■
16	Kutnahorite		●		●		
18	Tephroite	■	■				
19	Alleghanyite	●	●				
20	Ribbeite	■	■				
21	Spessartine			●	●	●	
22	Piemontite-Ce				×		
23	Rhodonite			●	●	●	●
24	Pyroxmangite			■	■	■	■
25	Caryopilite	●	■		●	■	
26	Pyrosmalite	×	●	×			
27	Talc*		×			●	
28	Phlogopite*			×			
29	Clinochlore*	●	●	●	●	●	●
30	Parsettensite			●	●	●	●
31	Neotocit	×	●				×
32	Apatite	×	×	×	×		

■ 1 ● 2 × 3

Fig. 2. Distribution of minerals in the oxide–carbonate–silicate manganese ore at the South Faizulino deposit. Minerals: (1) major (>5 vol %), (2) minor (1–5 vol %), (3) accessory (<1 vol %); Mn-bearing mineral species are denoted by an asterisk. Minerals were identified with optical methods, X-ray diffraction, electron microscopy, X-ray microprobe, and IR spectroscopy. [1] Quartz is detected as tiny (0.01 mm) inclusions in rhodochrosite spherulites. (*a–e*) Mineralic varieties of ore: (*a*) rhodochrosite–tephroite–ribbeite–hausmannite, (*b*) caryopilite–ribbeite–rhodochrosite–tephroite, (*c*) rhodochrosite–pyroxmangite, (*d*) rhodochrosite–pyroxmangite–quartz, (*e*) pyroxmangite–caryopilite–quartz; (*f*) rhodochrosite–pyroxmangite, quartz–pyroxmangite, and other veinlets.

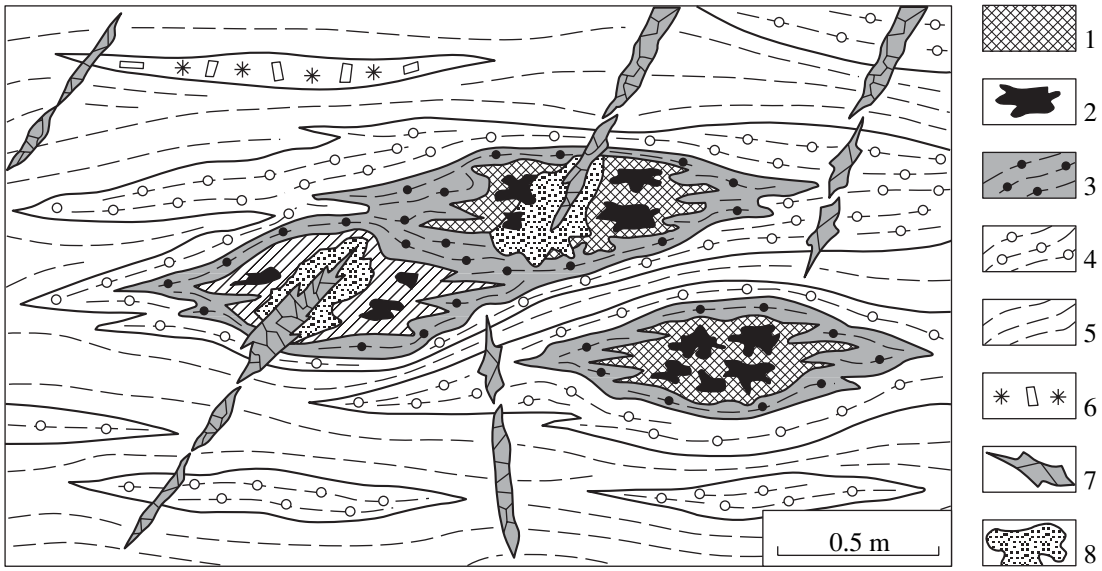

Fig. 3. Distribution of Mn ore varieties in the central part of the ore layer. Ore varieties in the main ore layer: (1, 2) rhodochrosite–tephroite–ribbeite–hausmannite: (1) rhodochrosite–tephroite mass, (2) ribbeite–hausmannite segregations; (3) caryopilite–ribbeite–rhodochrosite–tephroite; (4) rhodochrosite–pyroxmangite; (5) rhodochrosite–pyroxmangite–quartz; (6) pyroxmangite–caryopilite–quartz; (7, 8) zones of late veinlets: (7) pyroxmangite, (8) rhodochrosite.

The varieties listed above are distributed nonuniformly within the ore layer as a consequence of heterogeneous, lenticular–bedded, banded, and nodular structures of the initial Mn-bearing sediments (Fig. 3). The mineralogy of ore largely depends on the proportions of sharply dominating manganese and silicon; the occurrence of other components (Ti, Al, Fe, Mg, Ca, etc.) is recorded only in the minor and accessory phases.

The segments of the ore layer highly enriched in Mn are composed of hausmannite, ribbeite, tephroite, rhodochrosite, and caryopilite (varieties *a* and *b*). The ore with a lower Mn grade and a higher silicon content mainly consists of pyroxmangite, rhodochrosite, quartz, and caryopilite (varieties *c*, *d*, and *e*). All ore varieties are connected by gradual transitions. Hausmannite and then ribbeite and tephroite disappear consecutively with depletion in Mn and enrichment in Si (with decreasing Mn/(Mn + Si) ratio). Thereby, the percentage of caryopilite remains almost unchanged and the amount of rhodochrosite may even increase. In the course of a further decrease in the Mn/(Mn + Si) ratio, sporadic grains and small lenticular segregations of pyroxmangite appear and their number progressively increases. The rhodochrosite–pyroxmangite aggregates are formed in this way. Finally, quartz is added to pyroxmangite at the lowest Mn/(Mn + Si) ratio.

Hausmannite, ribbeite, and tephroite never occur in pyroxmangite- and quartz-bearing ores. However, the reverse situation is possible. Very small amounts of quartz were detected in Mn-rich varieties *a* and *b*. However, quartz is observed here only as tiny (0.01 mm) inclusions in rhodochrosite and is always isolated by carbonate from other minerals. Hausmannite, tephroite, and ribbeite never make up intergrowths with quartz and/or pyroxmangite. These minerals are always separated by rhodochrosite and caryopilite segregations.

Nevertheless, the relationships between mineral assemblages and Mn and Si contents at the South Faizulino deposit are not unequivocal and strict. The phase composition of ore may be different, changing from bed to bed, even at almost equal Mn /(Mn + Si) values. This is clearly seen from comparison of the observed mineral assemblages (Fig. 2) and the Mn–Si diagram (Fig. 4a), where the compositions of all major and some minor minerals were plotted together with the respective Mn/(Mn + Si) ratios in ore. For example, high Mn/(Mn + Si) ratios are characteristic not only of the ore consisting of hausmannite, ribbeite, and tephroite but also of some rhodochrosite–pyroxmangite and rhodochrosite–quartz ores. The rocks with low and almost equal Mn/(Mn + Si) values within a range of 0.18–0.25 also may be composed of three different assemblages: (1) pyroxmangite + quartz ± rhodochrosite, (2) rhodochrosite + quartz, and (3) caryopilite + quartz ± pyroxmangite. The first assemblage is most abundant at the deposit, while the two others are less frequent.

Thus, the correlation between the mineralogy and the chemical composition of ore in the main ore layer is traced as a clearly expressed tendency rather than a functional relationship.

Such a situation is typical of rocks metamorphosed at relatively low temperature and pressure. It is well known that under such conditions the formation of various mineral assemblages is controlled not only by the distribution of inert components in rocks but also by

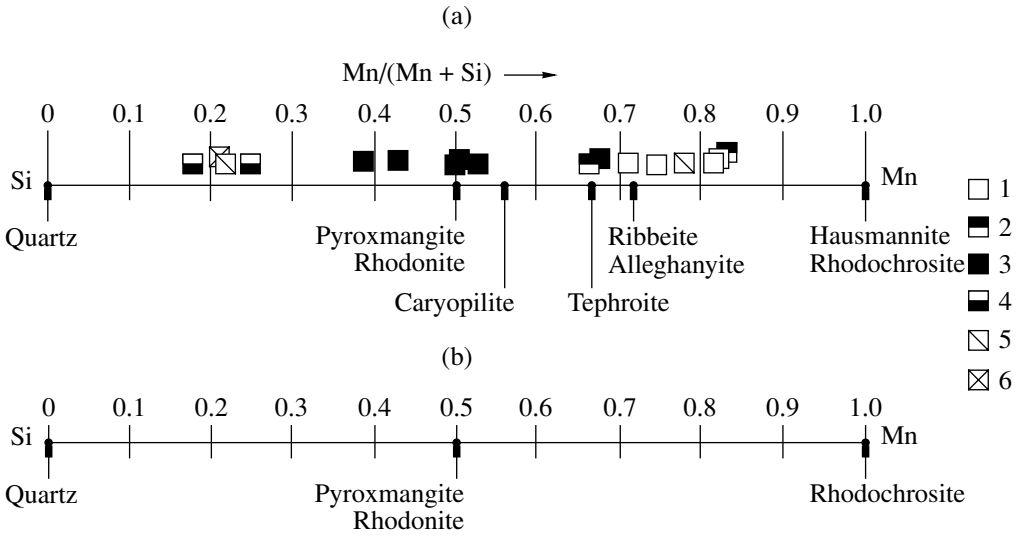

Fig. 4. Proportions of Mn and Si in minerals and manganese ore: (a) main ore layer and (b) late veinlets. Ore varieties: (1) rhodochrosite–tephroite–ribbeite–hausmannite; (2) caryopilite–ribbeite–rhodochrosite–tephroite; (3) rhodochrosite–pyroxmangite; (4) rhodochrosite–pyroxmangite–quartz; (5) rhodochrosite–quartz; (6) pyroxmangite–caryopilite–quartz.

other factors (Dobretsov et al., 1972; Logvinenko and Orlova, 1987). Kinetic constraints that suppress proceeding of reactions; the occurrence of finely dispersed phases, glass, and organic matter in sediments; local variations in admixtures in minerals; and the concentration of mobile components in pore fluid are of great importance. As a result of interaction of all these factors, rocks acquire variable and nonuniform mineralic compositions, which cannot be depicted completely in a composition–paragenesis diagram as is done traditionally for standard metamorphic rocks.

The vein complex. Crosscutting veinlets are developed locally at the deposit (Fig. 3). They are related to zones of the strongest tectonic deformation of the Mn-bearing layer and do not occur in the host cherty rocks beyond the orebody.

In contrast to the main body of ore, the late veinlets are very simple and uniform in composition of minerals, and their main assemblages are easily delineated in the Mn–Si diagram (Fig. 4b). Quartz–pyroxmangite, rhodochrosite–pyroxmangite, and rhodochrosite veinlets are prevalent; quartz–rhodonite, rhodochrosite–rhodonite, and monomineral pyroxmangite or quartz varieties are less frequent. The minor and accessory minerals are represented by calcite, Mn-clinochlore, parsettensite, neotocite, and arsenopyrite.

The veinlets are 0.3–5.0 cm thick and up to 50 cm long. Series of parallel or chaotically oriented veinlets are commonly formed.

According to relationships with the host ore, segregation and metasomatic veinlets are distinguished. The former occur in the ores with elevated silica contents (varieties *c*, *d*, and *e*). Their mineralogy fits the phase composition of host aggregates. The veinlets have clear straight boundaries and are composed of relatively large (as long as 5 mm), often perfectly faceted crystals that grew from selvages to the axis of the veinlet.

Metasomatic veinlets develop in the Mn-enriched segments of the ore layer composed of ribbeite, tephroite, rhodochrosite, and caryopilite (ore varieties *a* and *b*). Metasomatic veinlets have an uneven configuration with numerous juts. The zoning of veinlets is characterized by the development of a rhodochrosite or chlorite–rhodochrosite zone at the front of replacement and a pyroxmangite back zone. The mineral grains are oriented chaotically within each zone. In clusters of metasomatic veinlets, the protolith is often transformed into secondary rhodochrosite–pyroxmangite rock with zonal, taxitic, or stringer–reticulate structures. Metasomatic pyroxmangite veinlets without a clearly expressed carbonate rim occur only occasionally. In all cases, the mineralogy of metasomatic veinlets differs from the host aggregates.

Despite the different mechanisms of formation (segregation and metasomatic), the appearance of veinlets in both variants is caused by local redistribution of matter within the ore layer. The transfer of elements was provided by local pore solutions mobilized by tectonic movements. The migration of matter was limited to very short distances that do not exceed the thickness of the Mn-bearing layer. Nothing was supplied from external sources. The veinlets do not occur beyond the ore layer and are locally developed therein. Veinlets are small and have simple and uniform mineralic composition without phases that would be new for the deposit.

DESCRIPTION OF MINERALS

Hausmannite occurs only in the highest grade ore as relatively small (up to 2–4 cm across) microgranular

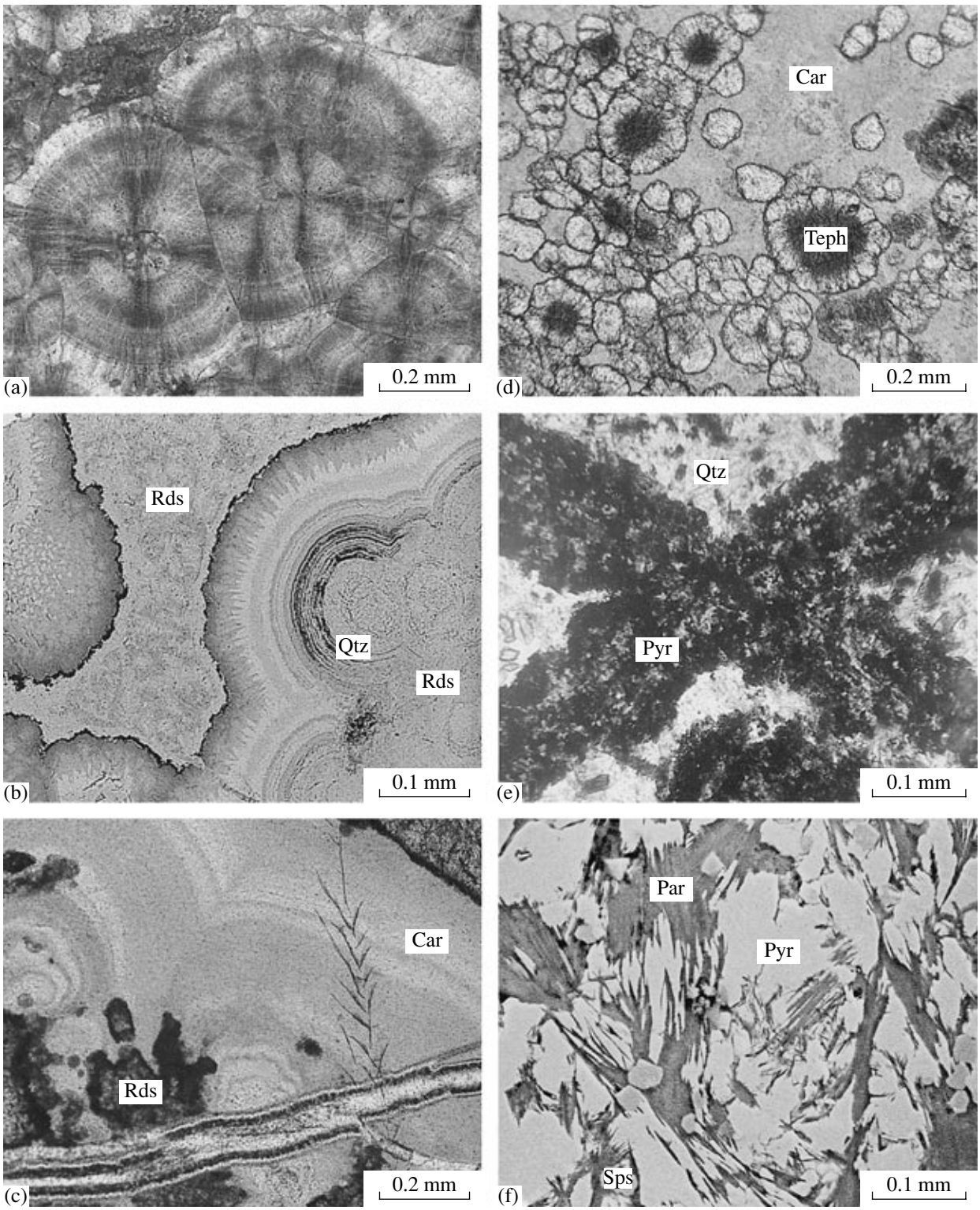

Fig. 5. Minerals of manganese ore at the South Faizulino deposit. (a, b) Rhodochrosite spherulites: (a) photomicrograph, crossed polars; (b) SEM photomicrograph; black zones are composed of quartz (Qtz), dark gray zones, of Ca-rich rhodochrosite (Rds), light gray zones, of Mn-rich rhodochrosite; the homogeneous gray mass consists of pelitic rhodochrosite; (c) concentrically zoned aggregate of caryopilite (Car) with inclusions of rhodochrosite I (dark spots) and a veinlet of rhodochrosite II, photomicrograph without analyzer; (d) tephroite segregations (Teph) in caryopilite mass (Car); dark areas in the center of tephroite segregations are composed of a microgranular aggregate overgrown by larger individuals of the outer zone, photomicrograph without analyzer; (e) intergrowth of tabular pyroxmangite crystals (Pyr), photomicrograph without analyzer; (f) spessartine (Sps) and parsettensite (Par) grains in pyroxmangite aggregate (Pyr), SEM photomicrograph.

(~0.01 mm) segregations irregular in shape. The hausmannite spots are severely corroded by rhodochrosite. In some places, the distribution of hausmannite relics clearly marks the bedded structure of the orebody; elsewhere, their orientation is random. Ribbeite and rhodochrosite commonly occur in intimate intergrowths with hausmannite.

Rhodochrosite is represented by two generations. The early rhodochrosite occurs in the main ore layer as microgranular, mosaic, pelitic, or spherulitic aggregates. The latter are most abundant at the deposit and the most interesting mode of rhodochrosite I occurrence (Figs. 5a, 5b). The particular spherulites are relatively large (0.3–2.0 mm in diameter) and made up of radiate threadlike individuals of rhodochrosite. As a rule, the spherulites reveal concentric zoning expressed in the rhythmic variation of Ca and Mn contents in carbonate and in the periodic appearance of very thin (~0.01 mm) quartz zones.

As can be clearly seen under a microscope, carbonate spherulites develop owing to the replacement of pelitic rhodochrosite, rhodochrosite + quartz, or silicate (neotocite, caryopilite) aggregates. The spherulites often occupy the whole rock and fragments of the protolith are retained only in the interstitial space between spherulites or the protolith is completely absent. The zoning of spherulites crystallized in the carbonate matrix is expressed only in the periodic oscillation of Mn and Ca contents, whereas additional quartz zones appear in spherulites that replace a quartz-bearing or silicate protolith.

The late rhodochrosite is a typical mineral of crosscutting veinlets, where it is represented by two morphological types: (1) the microgranular aggregate that is formed in the outer zones of metasomatic rhodochrosite–pyroxmangite veinlets and (2) xenomorphic grains that fill the space between tabular pyroxmangite or rhodonite crystals in axial zones of segregation veinlets.

By chemical composition (Table 1), rhodochrosite from different ore varieties is virtually indistinguishable. The range of Mn contents in the early rhodochrosite associated with hausmannite, ribbeite, and tephroite is somewhat narrower than in rhodochrosite I in association with pyroxmangite and quartz (87–98 and 73–98 mol % $MnCO_3$, respectively). The Mn and Ca contents in concentrically zoned rhodochrosite spherulites vary irregularly from one growth zone to another. The scatter of the Mn/(Mn + Ca) ratio in one rhodochrosite crystal may cover the entire possible compositional range of this mineral established at the deposit as a whole. The major element contents in the late rhodochrosite also vary widely; however, a correlation between the carbonate content in veinlets and their host rocks could not be established.

Kutnahorite commonly occurs as small (5–15 mm across) irregularly shaped fine-grained segregations among early spherulitic rhodochrosite aggregates or rhodochrosite–quartz rock. Isometric kutnahorite grains in the veinlets that crosscut these aggregates are much less abundant. The chemical composition of kutnahorite from the main ore layer and the late veinlets is virtually the same (Table 1) and differs from the theoretical composition $CaMn(CO_3)_2$ by a higher Ca content. On the basis of the Mn/(Mn + Ca) ratio, which equals 0.30–0.35, such a carbonate should be named manganese calcite. However, the X-ray pattern of the analyzed mineral differs in location of peaks and their intensity from calcite (ASTM 5-586) and corresponds precisely to kutnahorite (ASTM 19-234, 43-695). The main lines of the powder pattern of kutnahorite from the South Faizulino deposit are as follows: 3.79/25, 2.97/100, 1.435/15, 2.227/35, 2.063/12, 1.864/12, and 1.838/25 *d*(Å)/*I*. It cannot be ruled out that the increased Ca contents in the studied kutnahorite are caused by micrometer-size ingrowths of calcite.

Calcite at the deposit is a rare phase. In the main ore layer, calcite is represented by sporadic isometric grains dispersed through rhodochrosite aggregates. Calcite of the second generation occurs in the late veinlets as tabular or irregularly shaped grains. The composition of the mineral is uniform, with 95–98 mol % $CaCO_3$ and 1–4 mol % $MnCO_3$.

Tephroite is mainly related to the caryopilite interlayers and lenses. Rounded (up to 1 mm in diameter), radiate intergrowths of three to six thick tabular crystals are the typical mode of tephroite occurrence. The internal structure of such aggregates bears obvious indications of individual growth from center to periphery as in classic nodules. The tephroite micronodules crystallized replacing the caryopilite groundmass. Isolated nodules are relatively rare, and large segregations are most frequent. As the number of segregations increases, the amount of the cementing caryopilite decreases to complete disappearance (Fig. 5d). Further, the rock gradually becomes granoblastic as a result of recrystallization of tephroite, and the initial nodules are not retained. In addition to radiate segregations, tephroite forms narrow (0.3–1.0 mm thick) parallel rodlike rims at the boundary between ribbeite (alleghanyite) segregations and caryopilite.

The crystallization of tephroite is occasionally accompanied by the appearance of pyrosmalite occurring either as tabular crystals ingrown into tephroite and oriented largely along the nodule radii or in the mass of felted caryopilite in close proximity to the tephroite grains.

The chemical composition of tephroite is close to the theoretical composition of this mineral (Table 2). The X-ray pattern corresponds to the standard (ASTM 35-748). The parameters of the lattice unit (Å) are a = 4.890(3), b = 10.59(1), and c = 6.244(3).

Ribbeite and *alleghanyite* as polymorphic modifications of the chemical compound $Mn_5(SiO_4)_2(OH)_2$ are typical constituents of Mn-rich rocks. Together with hausmannite and rhodochrosite, these minerals make up small (5–20 mm across) light beige aggregates of

Table 1. Chemical composition of carbonates from the South Faizulino deposit, wt %

Component	Mineral															
	Rds I											Rds II		Kut I	Kut II	Cal I
	a	*b*	*c*	*c*	*c*	*c*	*c*	*c*	*c*	*d*	*e*	*f*(*b*)	*f*(*d*)	*d*	*f*(*d*)	*c*
	1	2	3	4	5	6	7	8	9	10	11	12	13	14	15	16
FeO	0.00	0.02	0.00	0.00	0.00	0.00	0.00	0.00	0.23	0.00	0.00	0.28	0.00	0.00	0.00	0.00
MnO	61.19	57.88	56.49	53.82	51.41	54.18	61.13	53.16	60.72	60.46	54.88	48.16	60.95	23.70	20.63	3.12
MgO	0.00	0.00	0.96	1.03	0.87	1.52	0.21	0.81	0.00	0.00	1.57	2.24	0.00	0.63	1.01	0.56
CaO	0.81	3.10	3.55	5.65	5.52	5.41	0.66	6.92	1.06	0.94	4.05	9.19	1.05	34.61	36.35	52.32
$CO_2^{(calcd)}$	38.60	38.35	38.88	38.95	39.04	39.51	38.67	39.30	38.64	38.25	38.94	39.71	38.64	42.32	42.44	43.61
Total	100.60	99.35	99.88	99.45	99.84	100.61	100.67	100.20	100.64	99.65	99.44	99.58	100.64	100.96	100.44	99.61
End members, mol %																
$FeCO_3$	0	0	0	0	0	0	0	0	0	0	0	0	0	0	0	0
$MnCO_3$	98	94	90	86	87	85	98	84	98	97	88	76	98	35	30	4
$MgCO_3$	0	0	3	3	2	4	1	2	0	0	4	6	0	2	3	1
$CaCO_3$	2	6	7	11	11	11	1	14	2	2	8	18	2	64	67	95

Note: Analyses were performed at the Laboratory of Electron Microscopy and Microanalysis of Mekhanobr-Analit Company, St. Petersburg, on a Camscan-4DV scanning electron microscope equipped with a Link-10000 spectrometer (Great Britain); analysts Yu.L. Kretser and A.I. Brusnitsyn. $CO_2^{(calcd)}$ is the calculated CO_2 content. Minerals: (Rds) rhodochrosite, (Kut) kutnahorite, (Cal) calcite; I and II are generations of minerals. Here and in Table 2: (*a*–*e*) mineralic varieties of manganese ore: (*a*) rhodochrosite–tephroite–ribbeite–hausmannite, (*b*) caryopilite–ribbeite–rhodochrosite–tephroite, (*c*) rhodochrosite–pyroxmangite, (*d*) rhodochrosite–pyroxmangite–quartz, (*e*) pyroxmangite–caryopilite–quartz; (*f*) rhodochrosite–pyroxmangite (rhodonite), quartz–pyroxmangite (rhodonite), and pyroxmangite (rhodonite) veinlets. The ore variety that hosts the veinlet is indicated in parentheses. Analyses 3–8 correspond to different zones of one spherulite (from inner to outer zones).

Table 2. Chemical composition of Mn silicates from the South Faizulino deposit, wt %

Component	Mineral													
	Teph	Rib	All	Sps		Pyr I		Pyr II		Rdn I	Rdn II	Car		
	b	*b*	*b*	*c*	*e*	*c*	*c*	*f*(*c*)	*f*(*b*)	*d*	*f*(*d*)	*a*	*b*	*b*
	1	2	3	4	5	6	7	8	9	10	11	12	13	14
SiO_2	30.49	24.51	24.89	36.80	37.03	46.78	46.37	46.24	46.80	46.70	46.76	34.80	35.62	37.33
Al_2O_3	0.39	0.19	0.12	21.03	20.89	0.00	0.00	0.00	0.00	0.00	0.00	2.81	0.41	1.23
FeO^{tot}	0.00	0.08	0.04	1.62	1.84	2.32	0.00	0.00	0.47	0.00	0.00	0.98	0.32	0.14
MnO	68.36	71.11	71.03	38.56	36.91	47.00	51.57	52.73	49.55	48.05	48.48	47.87	51.50	48.83
MgO	0.92	0.46	0.77	0.00	0.00	1.42	0.71	0.59	1.32	0.57	0.85	3.25	0.84	3.03
CaO	0.00	0.00	0.00	2.04	3.73	2.63	1.61	0.63	2.05	4.79	4.11	0.00	0.00	0.00
Total	100.16	96.35	96.85	100.05	100.40	100.15	100.26	100.19	100.19	100.11	100.20	89.71	88.69	90.56
(O)*	4	9	9	12		3						13		
Formula units														
Si	1.01	2.00	2.01	3.00	3.01	1.00	1.00	1.00	1.00	1.00	1.00	3.75	3.95	3.94
Al	0.01	0.02	0.01	2.03	2.00	0.00	0.00	0.00	0.00	0.00	0.00	0.36	0.05	0.14
Fe^{2+}	0.00	0.01	0.00	0.11	0.12	0.04	0.00	0.00	0.01	0.00	0.00	0.03	0.03	0.02
Mn	1.92	4.91	4.86	2.67	2.54	0.85	0.94	0.97	0.90	0.87	0.88	4.36	4.84	4.40
Mg	0.05	0.06	0.09	0.00	0.00	0.05	0.02	0.02	0.04	0.02	0.03	0.52	0.14	0.48
Ca	0.00	0.00	0.00	0.18	0.32	0.06	0.04	0.01	0.05	0.11	0.09	0.00	0.00	0.00
Total	2.99	7.00	6.97	7.99	7.99	2.00	2.00	2.00	2.00	2.00	2.00	9.02	9.01	8.97

Table 2. (Contd.)

Component	Mineral													
	Car		Prm	Tlc	Cch I				Cch II			Par I	Par II	Neo II
	e	*e*	*c*	*e*	*a*	*c*	*e*	*e*	*f*(*b*)	*f*(*b*)	*f*(*b*)	*c*	*d*	*f*(*b*)
	15	16	17	18	19	20	21	22	23	24	25	26	27	28
SiO_2	38.00	36.12	35.72	61.75	30.17	28.42	31.04	29.62	30.80	32.17	32.17	46.00	4.74	45.15
Al_2O_3	2.49	4.07	0.80	0.00	19.34	18.92	15.42	18.31	15.19	17.42	13.92	4.01	3.80	0.00
FeO^{tot}	6.71	8.28	0.97	6.34	1.08	8.51	13.62	13.51	1.67	3.74	11.59	3.29	3.12	0.00
MnO	37.54	34.95	48.97	2.39	12.42	8.72	6.08	4.52	17.72	6.75	6.54	30.37	29.36	42.21
MgO	6.03	6.21	2.49	25.65	26.55	23.66	22.32	22.35	23.27	28.25	23.45	2.93	3.31	0.77
CaO	0.00	0.00	0.00	0.00	0.00	0.00	0.00	0.00	0.00	0.00	0.00	0.65	1.04	0.00
K_2O	0.00	0.00	0.00	0.00	0.00	0.00	0.00	0.00	0.00	0.00	0.00	1.68	2.51	0.24
Total	90.77	89.62	88.95	96.13	88.56	88.24	88.51	88.30	88.65	88.33	87.67	89.21	87.02**	88.37
(O)*	13		20	11	14							27		3
Formula units														
Si	3.90	3.75	6.01	4.02	2.94	2.84	3.12	2.96	3.09	3.08	3.24	9.29	9.12	1.06
Al	0.30	0.50	0.16	0.00	2.11	2.23	1.83	2.16	1.80	1.97	1.65	0.95	0.93	0.00
Fe^{2+}	0.57	0.72	0.14	0.34	0.09	0.71	1.15	1.13	0.14	0.30	0.98	0.56	0.54	0.00
Mn	3.26	3.07	6.98	0.13	1.02	0.74	0.52	0.38	1.51	0.55	0.56	5.20	5.19	0.84
Mg	0.92	0.96	0.62	2.49	3.85	3.53	3.35	3.33	3.48	4.04	3.52	0.88	1.03	0.03
Ca	0.00	0.00	0.00	0.00	0.00	0.00	0.00	0.00	0.00	0.00	0.00	0.14	0.23	0.00
K	0.00	0.00	0.00	0.00	0.00	0.00	0.00	0.00	0.00	0.00	0.00	0.42	0.67	0.01
Total	8.95	9.00	13.91	6.98	10.01	10.05	9.97	9.96	10.02	9.94	9.95	17.44	17.77**	1.94

Note: Analyses were performed at the Laboratory of Electron Microscopy and Microanalysis of Mekhanobr-Analit Company, St. Petersburg, on a Camscan-4DV scanning electron microscope equipped with a Link-10000 spectrometer (Great Britain); analysts Yu.L. Kretser and A.I. Brusnitsyn. (O*) Number of oxygen atoms in calculation of crystallochemical formulas. ** 0.15 wt % Na_2O was detected in analysis of parsettensite; this value corresponds to 0.06 f.u.; these figures were added to total oxides and cations. Minerals: (Car) caryopilite, (Rib) ribbeite, (Äll) alleghanyite, (Teph) tephroite, (Pyr) pyroxmangite, (Rdn) rhodonite, (Sps) spessartine, (Cch) clinochlore, (Par) parsettensite, (Tlc) talc, (Prm) pyrosmalite, (Neo) neotocite. I and II are generations of minerals. Analyses 10 and 11, 13, and 14 correspond to pairs of minerals from the main ore layer and crosscutting veinlets in two samples: (10, 11) substantially pyroxmangite ore, (13, 14) substantially rhodonite ore.

diverse morphology: colloform, globular, or flakelike. The minerals look similar in transmitted light: they are light pinkish beige in color without pleochroism; $N_m \approx 1.75$, $N_g - N_p \approx 0.035$. The chemical composition of the minerals is given in Table 2. Thorough study has shown that ribbeite is a major mineral at the deposit, while alleghanyite is a minor mineral. The minerals often occur jointly. The main lines of the X-ray pattern of ribbeite are as follows: 4.42/25, 3.85/25, 3.57/15, 3.38/17, 3.94/55, 2.87/100, 2.80/20, 2.71/55, 2.69/40, 2.56/55, 2.53/40, 2.42/20, 2.36/35, and 2.33/13 *d*(Å)/*I*. The following reflections are diagnostic for alleghanyite: 3.62/70, 3.15/40, 2.86/100, 2.78/32, 2.74/38, 2.71/38, 2.70/50, 2.69/32, 2.61/60, 2.55/30, 2.54/20, 2.44/32, 3.39/36, 2.36/45, and 2.35/25 *d*(Å)/*I*. The detailed characteristics of ribbeite and alleghanyite were given by Brusnitsyn and Chukanov (2002).

Spessartine occurs as small (0.01–0.02 mm across) isometric, often euhedral grains mainly related to segregations of clinochlore and parsettensite (Fig. 5f). The optic properties and X-ray pattern of the mineral are standard. Spessartine always contains appreciable amounts of Ca and Fe (Table 2).

Pyroxmangite and *rhodonite* belong to a group of manganese pyroxenoids having very similar diagnostic properties. The exact identification of the minerals is feasible only with X-ray patterns. The use of this method has shown that pyroxmangite is predominant at the South Faizulino deposit, whereas rhodonite is a minor mineral; they may occur jointly.

Let us consider the mode of occurrence of pyroxenoids as exemplified in pyroxmangite. Two generations of this mineral are clearly recognized. Pyroxmangite I occurs in the main ore layer as radiate, cross-shaped, and formless intergrowths of small (0.2–0.5 mm) tabular or isometric crystals. The grains of early pyroxmangite often are poorly crystallized; they have uneven outlines and a mosaic, microblock structure with local isotropic areas. Numerous inclusions of quartz, rhodochrosite, caryopilite, spessartine, chlorite, and some other earlier minerals are observed (Fig. 5e). Pyroxmangite II forms crosscutting veinlets. In contrast to pyroxmangite I, defective individuals are untypical. Conversely, relatively large (up to 5 mm long) and often perfectly faceted crystals of tabular and flattened habits make up fanlike, columnar, or parallel rodlike aggregates. A similar morphology is characteristic of rhodonite.

The X-ray patterns of pyroxmangite and rhodonite are best distinguishable in the range 3.60–2.50 Å, where the following reflections are recorded for pyroxmangite: 3.43/15, 3.33/17, 3.18/20, 3.13/45, 3.03/30, 3.00/35, 2.96/100, 2.67/35, 2.65/20, and 2.61/30 *d*(Å)/*I*. The diagnostic peaks of rhodonite are 3.56/40, 3.33/45, 3.14/55, 3.09/48, 2.96/100, 2.94/80, 2.76/50, 2.65/20, and 2.60/25 *d*(Å)/*I*.

Pyroxenoids from the South Faizulino deposit are different in Ca contents, which are twice as high in rhodonite as in pyroxmangite (Table 2).

Caryopilite is a Mn phyllosilicate $Mn_5(Si_4O_{10})(OH)_6$ with a structure close to the structure of antigorite (Guggenheim and Eggleton, 1998). At the South Faizulino deposit, this mineral occurs as small (3–15 mm thick) interlayers, lenses, or irregular segregations in ores of various compositions. The caryopilite aggregates have pelitic, felted, colloform, globular, or concentric rhythmically zoned structures identical to the structure of crystallized gel or glass (Fig. 5c). The cracks of syneresis are often observed in the caryopilite matrix; fusiform or threadlike rhodochrosite grains are related to these cracks. Microgranular caryopilite occasionally contains small (~0.2 mm across) relict inclusions of isotropic glassy neotocite.

The chemical composition of caryopilite is characterized by variable contents of admixtures (Table 2). The Al, Fe, and Mg contents in caryopilite associated with ribbeite, tephroite, and rhodochrosite are relatively low; their total content is not higher than 15% of the bulk of cations. In caryopilite from intergrowths with pyroxmangite and quartz, the contents of admixtures (Fe and Mg above all else) are much higher and amount to 35–40% of cation totals. Such caryopilite is close in composition to *gonyerite*—a Mn mineral from the chlorite group. However, its X-ray pattern corresponds to the serpentine-like structure of polytype 1M, whereas the peak with $d \approx 14$ Å characteristic of chlorites is absent. The most intense reflections in the X-ray pattern of caryopilite enriched in Mg and Fe (Table 2, an. 15) are as follows: 7.23/98, 3.619/75, 3.580/47, 2.790/82, 2.501/100, 2.360/12, 2.087/38, 1.974/12, 1.725/10, 1.632/25, 1.621/25, and 1.590/18 *d*(Å)/*I*. The unit cell parameters (Å) are $a = 5.619(2)$, $b = 9.770(3)$, $c = 7.477(3)$, and $\beta = 104.70(4)°$. Caryopilite with lower contents of admixtures (Table 2, an. 14) differs by smaller dimensions of the unit cell (Å): $a = 5.683(4)$, $b = 9.795(5)$, $c = 7.535(5)$, and $\beta = 104.15(6)°$.

Pyrosmalite $Mn_8(Si_6O_{15})(OH)_{10}$ mainly concentrates in the caryopilite–ribbeite–rhodochrosite–tephroite ore. Tabular crystals of pyrosmalite up to 0.3 mm long are observed largely in caryopilite lenses in close intergrowths with tephroite "nodules" or occurring nearby. Pyrosmalite was also identified as felted aggregates associated with kutnahorite. In transmitted light, the mineral is colorless or, occasionally, pale yellow; pleochroism is extremely weak; cleavage in one direction is perfect; extinction is parallel; $N_m \approx 1.65$, $N_g - N_p \approx 0.030$.

The X-ray pattern of the studied mineral is close in intensity and localization of most peaks to the standard pattern for pyrosmalite (ASTM 12-268; Guggenheim and Eggleton, 1988) and differs from the X-ray patterns of Mn silicates similar in structure and composition (caryopilite, bementite, and friedelite). The main lines are as follows: 7.20/80, 4.48/10, 3.78/25, 3.55/45, 3.34/10, 2.65/100, 2.25/45, 1.838/30, 1.649/20, and 1.632/20 *d*(Å)/*I*. At the same time, several reflections are not always developed clearly in our X-ray patterns:

11.5/20, 6.06/30, 4.87/20, 4.35/20, and 3.41/40 *d*(Å)/*I*. Most likely, this is caused by a low concentration of pyrosmalite in our samples and by superposition of its peaks upon peaks of kutnahorite, rhodochrosite, and other minerals and by partial texturing of specimens. The chemical composition of pyrosmalite (Table 2) is characterized by insignificant contents of Al, Fe, and Mn admixtures.

Talc occurs in intimate association with spessartine and clinochlore. Small (up to 0.3 mm long) tabular individuals of talc are either nonuniformly dispersed through the chlorite matrix or are gathered into sheaflike and parallel rodlike aggregates. Under a microscope, the mineral is colorless, devoid of pleochroism, and has parallel extinction; $N_m \approx 1.60$, $N_g - N_p \approx 0.040$. Talc is clearly recorded in X-ray patterns by the three strongest reflections: 9.29/50, 4.67/30, and 3.12/100 *d*(Å)/*I*. The chemical composition of talc is given in Table 2.

Manganese clinochlore, one of the most abundant minor minerals in the studied rocks, is represented by two generations. Clinochlore I commonly occurs as small (up to 5 mm across) fine flaky, radiate, and parallel fibrous aggregates that fill interstitial spaces between rhodochrosite spherulites and rhodonite and quartz crystals. Clinochlore II fills the late veinlets.

The X-ray pattern of the mineral is close to the standard of Mn-free clinochlore 1M (ASTM 7-165, 12-242, 29-701). The main lines of the X-ray pattern of chlorite (Table 2, an. 24) are as follows: 14.29/40, 7.11/75, 4.738/60, 3.550/100, 2.840/55, 2.585/20, 2.542/30, 2.445/22, 2.387/22, 2.262/15, 2.001/30, 1.564/15, and 1.540/25 *d*(Å)/*I*. The unit cell parameters (Å) are a = 5.349(1), b = 9.244(2), c = 14.312(1), and β = 97.11(2)°.

According to the modern nomenclature (Strunz and Nickel, 2001), the chemical composition of the mineral (Table 2) corresponds to manganese clinochlore. In terms of the obsolete classification (Hey, 1954; *Minerals…*, 1992), most of the analyses also fit this mineral species, but two analyses fall into the pennine field according to silicon contents.

Clinochlore from different mineral assemblages is not uniform in composition. The lowest Fe contents are established in the ore varieties enriched in Mn and in some substantially rhodochrosite areas of the rhodochrosite–pyroxmangite ore. Elsewhere, the Fe content in clinochlore is more than three times higher. This specific feature is characteristic of clinochlore from both the main ore layer and the crosscutting veinlets. No distinct systematic patterns were established in the distribution of other cations.

Parsettensite $KMn_7[(Si_9Al)O_{24}](OH)_6 \cdot nH_2O$ is a K-bearing Mn phyllosilicate. In the main ore layer, parsettensite I occurs as sheaflike, radiate, and star-shaped intergrowths of sheetlike micaceous crystals and as microgranular felted aggregates (Fig. 5f). In the late veinlets, parsettensite is represented by relatively large (up to 3 mm long) sheets.

The main lines in the X-ray pattern of this mineral are as follows: 12.5/100, 6.32/17, 4.49/10, 4.16/22, 3.68/20, 3.12/20, 2.78/30, 2.63/40, 2.41/20, and 2.15/10 *d*(Å)/*I*. The chemical composition of parsettensite (Table 2) is little different from the data reported from other deposits.

Neotocite is an X-ray amorphous Mn silicate that approximately corresponds to the formula $Mn(SiO_3) \cdot H_2O$ (Clark et al., 1978). In the studied ore, neotocite occurs in caryopilite aggregates from the main ore layer and in the late veinlets. In the first case, it is rather large (commonly 0.2 mm and up to 2 cm across) irregular relict inclusions replaced by felted caryopilite. In the second case, neotocite fills the interstitial space between pyroxmangite, rhodochrosite, and quartz crystals in axial zones of veinlets. The mineral has a very characteristic glassy appearance. In samples, neotocite is dark reddish brown; the luster is greasy; the mineral is brittle; and the fracture is shell-like. Under a microscope, neotocite is light brown and isotropic; n = 1.520. The mineral is reliably identified with IR spectroscopy. The main bands of the IR spectrum are as follows: 454, 618, 659, 780, 1015, 1633, 325, 3420, and 3640 cm^{-1}.

DISCUSSION

As has been shown previously, the ore layer of the South Faizulino deposit is hydrothermal–sedimentary in origin (Brusnitsyn and Zhukov, 2005). The manganese mud accumulated at the active continental margin during a period of waning volcanic activity. The ore matter was supplied into the marine basin by hydrothermal solutions that were circulating through the oceanic crust and precipitated on the bottom near the vents. Manganese in all probability precipitated in oxide form as takes place in modern hydrothermal systems. In addition, silica, clay, and other minerals were present in the sediment. At the diagenetic stage and during further transformations, the mineralic composition of Mn-bearing sediment underwent substantial changes. The data presented in this paper make it possible to reconstruct the mineral formation during the burial of manganese ore and the subsequent tectonic rearrangement of the region.

The mineral formation at the stage of burial of manganese ore layers. The relationships between minerals in the main ore layer indicate that, with increasing temperature and pressure, the formation of different mineral assemblages was controlled largely by the initial composition of sediments.

First of all, the mode of occurrence and morphology of hausmannite grains attract attention. This mineral occurs as cavernous segregations irregular in shape and actively corroded by rhodochrosite. Such aggregates likely are the metamorphosed relics of primary sedi-

mentary Mn oxides and/or hydroxides partly replaced with carbonate.

As is known, finely dispersed oxides of tri- and quadrivalent manganese (todorokite, birnessite, rancieite, etc.) are the main species of Mn accumulation in marine hydrothermal deposits. In the course of diagenesis and at advanced stages of lithogenesis, the depletion of pore solution in oxygen, along with increasing temperature and pressure, gives rise to the reduction of manganese, so that primary oxides and hydroxides are transformed into other minerals. Manganite and pyrolusite crystallize most often in slightly altered sedimentary ore, whereas hausmannite is most abundant in carbonate-bearing metamorphosed rocks.

During the burial of ore, the Mn oxides were replaced with rhodochrosite. Most likely, carbonation of sediment proceeded most intensely at the stage of diagenesis, when the concentration of oxygen in pore solution dropped as a result of organic matter oxidation, while the concentration of carbon dioxide increased.[3]

The diagenetic origin of rhodochrosite is indicated by its morphology. The bulk of this mineral is represented by spherulites of threadlike crystals that grew in a fine-grained carbonate or silicate matrix. Such spherulites most likely postdated the ore matter sedimentation. Metamorphism is also not favorable for the growth of threadlike individuals because long-term heating results in recrystallization of carbonate needles into larger grains. Spherulites commonly grow in a viscous (colloidal) medium at a great oversaturation of the mineral-forming solution (Krasnova and Petrov, 1997). Diagenesis is the most suitable process in this respect. The rhodochrosite spherulites in the manganese ore at the Obrochishte deposit in Bulgaria, the formation of which was completed exactly at the diagenetic stage (Aleksiev, 1960), are identical to those known from the southern Urals. In all probability, the carbonate spherulites at the South Faizulino deposit also are of diagenetic origin and their good preservation is a result of low metamorphic grade.

Rhodochrosite often replaces Mn oxides completely. However, where the entire resource of carbon dioxide was consumed in the course of carbonation, an excess of manganese could have been retained in the oxide form as hausmannite. Furthermore, low contents of silica and/or clay minerals are necessary for the retention of Mn oxides; otherwise, oxides would be transformed into silicates. It is hardly accidental that hausmannite segregations at the South Faizulino deposit occur only in the ore with the highest Mn grade and low concentrations of other components. In all other cases, the oxides are completely replaced with rhodochrosite and silicates.

A wide spread of globular, colloform, concentrically zoned, and other structures typical of gel or glass crystallization is characteristic of the studied ore. Such structures are especially typical of caryopilite aggregates. The cracks of syneresis are abundant in these aggregates, and relics of the glassy protolith (neotocite) are observed in the main ore layer. The admixture of Al and Mg, elements that are untypical of Mn oxides and silicates, is also in line with this interpretation.

While discussing the formation conditions of caryopilite, it is expedient to dwell on the genesis of the earlier neotocite. This mineral was identified in Mn ore of various origins (Clark et al., 1978; Roy, 1981; *Minerals*..., 1992). Neotocite often occurs in unmetamorphosed manganese ore layers, where it is considered to be a product of coagulation of Mn silicate gel within sediments. Neotocite as a parental Mn–Si gel-like phase is very unstable and may be retained only at a low carbon dioxide concentration in pore solution. Otherwise, neotocite is readily replaced with rhodochrosite, including spherulites of this mineral, and opal. Diagenetic neotocite was described in detail at the Obrochishte deposit in Bulgaria (Aleksiev, 1960) and the Chkhikvta deposit in Georgia (Andrushchenko et al., 1985). In addition to these localities, neotocite was mentioned in some areas of the Nikopol deposit in Ukraine, the Chiatura deposit in Georgia, the Polunochny deposit in Russia, etc.

Keeping these data in mind, it is suggested that a Mn–Si gel-like phase did occur in ore-bearing sediments at the South Faizulino deposit.

At the stage of diagenesis, the gel was partly replaced by rhodochrosite spherulites and its retained fragments were transformed into neotocite. A further rise in temperature and pressure resulted in the transformation of neotocite into caryopilite.

The transition of neotocite into caryopilite was accompanied by the release of silica:

$$5Mn(SiO)_3 \cdot H_2O \longrightarrow Mn_5(Si_4O_{10})(OH)_6 + SiO_2 + 2H_2O. \quad (1)$$

With increasing temperature and pressure, the free silica reacted with caryopilite with formation of pyroxmangite or rhodonite according to the reaction

$$Mn_5(Si_4O_{10})(OH)_6 + SiO_2 \longrightarrow 5Mn(SiO_3) + 3H_2O. \quad (2)$$

The assemblage of caryopilite and quartz becomes unstable already at the conditions of the prehnite–pumpellyite facies. However, as the study of the South Faizulino deposit has shown, this is valid only in respect to caryopilite with a low concentration of admixtures. Caryopilite enriched in Al, Fe, and Mg and approaching gonyerite in composition may form intimate intergrowths with quartz without any indication of

[3] Participation of oxidized biogenic hydrocarbons in the formation of rhodochrosite is supported by the carbon isotopic composition (Kuleshov and Brusnitsyn, 2004). The reducing conditions created at the stage of diagenesis were also retained at the subsequent stages of mineral formation and promoted the crystallization of minerals of bivalent manganese.

corrosion at the same temperature and pressure. In all probability, the admixtures stabilize the serpentine-like structure of caryopilite and thus expand the field of its stability toward higher temperatures, whereas caryopilite with low Al, Fe, and Mg contents is very unstable. In addition to the interaction with quartz, some other transformations of caryopilite are typical. Crystallization of radiate tephroite intergrowths in the caryopilite matrix is clearly seen under a microscope. This process could have been realized as a result of interaction of caryopilite with finely dispersed rhodochrosite inclusions

$$Mn_5(Si_4O_{10})(OH)_6 + 3Mn(CO_3) \longrightarrow 4Mn_2(SiO_4) + 3H_2O + 3CO_2 \quad (3)$$

or by breakdown of caryopilite, e.g., as

$$5Mn_5(Si_4O_{10})(OH)_6 \longrightarrow 2Mn_2(SiO_4) + 3Mn_7(Si_4O_{10})(OH)_8 + 3H_2O, \quad (4)$$

where $Mn_7(Si_6O_{15})(OH)_8$ is bementite, a Mn phyllosilicate close to caryopilite in composition and crystal structure.

Bementite was not found at the South Faizulino deposit. By all diagnostic attributes, this mineral is similar to caryopilite. Therefore, it is hardly possible to identify bementite in the fine-grained samples with sharply prevalent caryopilite. Nevertheless, it cannot be ruled out that a small amount of bementite as a product of reaction (4) occurs in the studied samples.

Finally, according to petrographic studies, caryopilite is unstable in association with ribbeite. Tephroite is a product of the interaction between these minerals:

$$Mn_5(Si_4O_{10})(OH)_6 + 3Mn_5(SiO_4)_2(OH)_2 \longrightarrow 10Mn_2(SiO_4) + 6H_2O. \quad (5)$$

Ribbeite is an earlier mineral with respect to tephroite. Its formation conditions and polymorphic transformation into alleghanyite were considered by Brusnitsyn and Chukanov (2002).

The breakdown of caryopilite with formation of tephroite and presumably bementite (reaction (4)) has been reproduced experimentally. The experiments were carried out for 3 days in a reactor with a cold valve under 500 bars pressure of pure water at temperatures of 450, 400, 350, and 300°C. Caryopilite from the Kyzyltash deposit (the southern Urals) was chosen as a starting material; its chemical composition was close to the theoretical composition of this mineral ((wt %) 36.80 SiO_2, 0.96 Al_2O_3, 53.46 MnO, 91.23 in total). The mineralic composition of each sample before and after the run was determined with X-ray diffraction.

The breakdown of caryopilite and crystallization of tephroite were established in all runs, and the intensity of this process sharply increased with a rise in temperature. Thus, the upper temperature limit of stability of chemically pure caryopilite at $P = 0.5$ kbar is below 300°C. Because dehydration reactions commonly depend very little on pressure, the results obtained may be used to reconstruct the mineral formation conditions at the South Faizulino deposit, where the maximum pressure is estimated at 2.5 kbar.

In my opinion, the available observations quite convincingly indicate that neotocite and, afterwards, caryopilite, ribbeite, tephroite, pyrosmalite, and (partly) pyroxmangite (rhodonite) were formed as a result of transformation of material initially contained in the ore-bearing sediment as a gel-like Mn–Si phase. The nature of this protolith and the conditions of its formation so far remain poorly studied. However, the possibility of its existence has been noted by many researchers. In particular, such ideas regarding the genesis of caryopilite and orthosilicates (tephroite, alleghanyite, and sonolite) were proposed for the hydrothermal–sedimentary manganese deposits hosted in the Franciscan Group in California (Flohr and Huebner, 1992; Huebner et al., 1992).

The ore varieties enriched in silica are composed largely of quartz, rhodochrosite, pyroxmangite, and rhodonite. The relationships between these minerals are equivocal. In many places, fine intergrowths of rhodochrosite with quartz are observed; however, elsewhere, quartz and rhodochrosite do not make up a stable assemblage but react with each other to crystallize pyroxmangite or rhodonite:

$$MnCO_3 + SiO_2 \longrightarrow Mn(SiO_3) + CO_2. \quad (6)$$

The replacement of carbonate with pyroxenoids is especially evident in the banded ore. Rhodochrosite is locally retained therein only within the beds of newly formed pyroxmangite as isometric or irregularly shaped relics isolated from quartz. The pyroxmangite (rhodonite) crystals themselves contain numerous inclusions of both rhodochrosite and quartz.

Pyroxmangite and rhodonite could have formed not only as products of reaction of quartz with rhodochrosite (reaction (6)) but also as a result of other processes, for example, by interaction of quartz with caryopilite (reaction (2)) or Mn oxides. At an excess of SiO_2, the quartz–pyroxmangite (rhodonite) assemblage was formed in ore in all cases.

Pyroxmangite and rhodonite are silicates with very similar structure and chemical composition. At the South Faizulino deposit, they occur as grains similar in morphology and often as syngenetic intergrowths. Thereby, these minerals differ from each other by the Ca content, which is approximately twice as high in rhodonite. This implies that crystallization of Mn pyroxenoids was controlled by the distribution of Ca in rock. Pyroxmangite was formed in the ore layer segments with the lowest Ca content, while enrichment in Ca led to the appearance of rhodonite. Inasmuch as the Ca content in the ore at the South Faisulino deposit is low and does not exceed 2 wt % CaO on average,

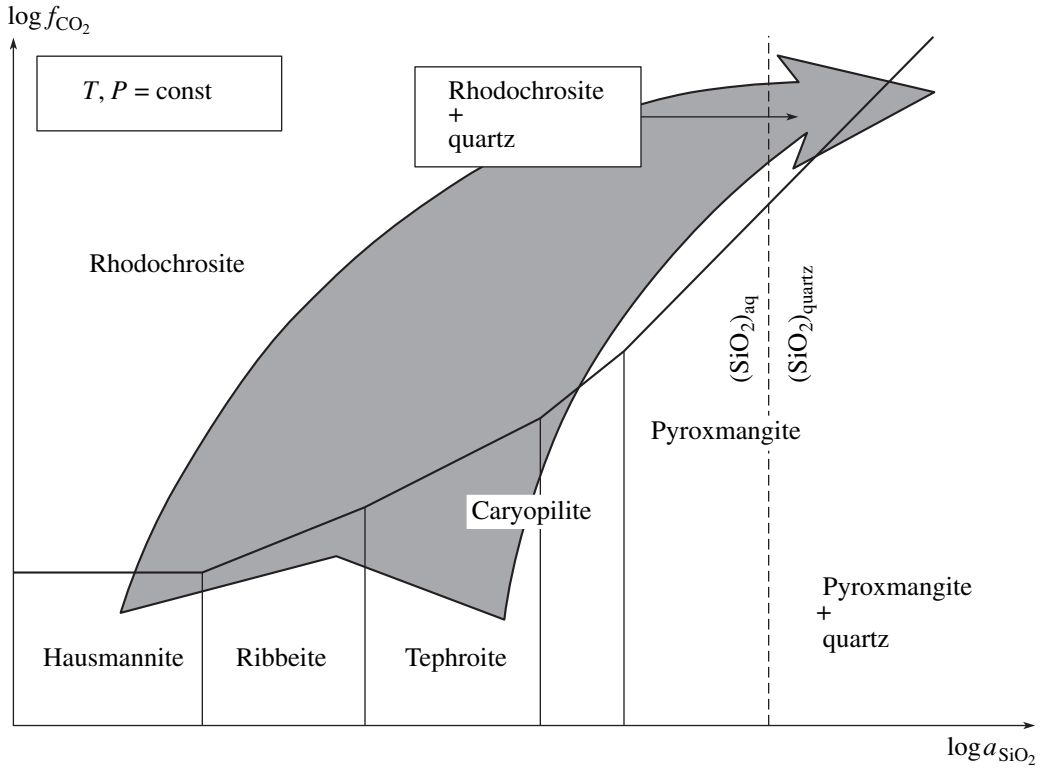

Fig. 6. Equilibria of Mn minerals depending on carbon dioxide fugacity and silica activity in solution. The arrow indicates the direction of change in solution composition in the process of metasomatic veinlet formation with separation of rhodochrosite frontal and pyroxmangite back zones in the rhodochrosite–tephroite–hausmannite ore.

pyroxmangite dominates at this deposit, whereas rhodonite is a minor mineral.

The quartz–pyroxmangite (rhodonite) assemblage with Mn clinochlore, spessartine, parsettensite, and talc is very characteristic of the studied deposit. Sporadic grains of pyrophanite, phlogopite, and piemontite-Ce occur in the same places. Such an assemblage of Mn and Si minerals with minerals of Al, Mg, and Ti is caused by the occurrence of a terrigenous clayey admixture in the initial ore-bearing sediment. As is known, the burial of clayey sediments results in the formation of hydrated phyllosilicates. In the South Faizulino ore, this is, first of all, chlorite and parsettensite. The crystallization of anhydrous spessartine (a Mn–Al mineral from the garnet group) is a specific feature of the manganese ore layers.

The experimental synthesis of spessartine as a product of the reaction between Mn chlorite and quartz has shown that, at a pressure of 0.5 kbar, garnet is formed at 340°C. The temperature of garnet formation rises to 400°C at 1 kbar and increases further by 10°C per kilobar (Hsu, 1968). However, the reverse reaction of spessartine breakdown could not be reproduced. Therefore the obtained estimates of the temperature of spessartine crystallization most likely should be regarded as overestimated relative to the equilibrium values.

In particular, according to the experimental data, the temperature of spessartine formation at a pressure of 2.5 kbar should be no lower than 410°C, i.e., more than 100°C higher than the highest possible temperature of metamorphism at the South Faizulino deposit. At the same time, spessartine is one of the most abundant minor minerals at the deposit. The mineral often occurs as perfectly faceted crystals that do not bear signs of a metastable state in their morphology and relationships with other minerals. Therefore, the formation of spessartine does not require such high temperatures as follow from the experimental results. Spessartine crystallization at a relatively low temperature (≈300°C) was also suggested by researchers of manganese deposits in Belgium, Ghana, California, and other regions (Flohr and Huebner, 1992; Theye et al., 1996; Nyame, 2001).

Mineral formation in veinlets. The veinlets that occur throughout the Mn ore lens are composed largely of pyroxmangite (rhodonite), rhodochrosite, and quartz; clinochlore, parsettensite, and some other minerals are much less abundant. With regard to mineral assemblages, the vein facies is identical to the rhodochrosite–pyroxmangite and rhodochrosite–pyroxmangite–quartz ores that are predominant at the deposit. It is evident that the veinlets were formed by the mechanism responsible for the formation of Alpine veins, where small cracks were sealed with a substance supplied with pore solutions from the host mineral aggregates.

At the same time, an additional gain of silica is required for the formation of the metasomatic pyroxmangite and rhodochrosite–pyroxmangite veinlets hosted in the Mn-enriched caryopilite–ribbeite–rhodochrosite–tephroite ore. Both the quartz-bearing varieties of the Mn ore itself and the cherty rocks that host the orebody might have served as a source of silica. The appearance of a rhodochrosite zone indicates an increase in the concentration of carbon dioxide, which likely was supplied from the adjacent segments of the ore layer. The compositional variation of the solution during the formation of metasomatic zonal veinlets is demonstrated in the $\log f_{CO_2} - \log a_{SiO_2}$ diagram (Fig. 6). As can be seen, the CO_2 fugacity increases first and afterwards the silica activity starts to grow. This sequence of events reflects a higher mobility of SiO_2 in comparison with silica.

Furthermore, the mineralogical uniformity of veinlets, established for the entire extent of the ore layer, probably indicates that a network of periodically opening fissures functioned as a system of communicating vessels, where possible local differences in fluid composition were rapidly leveled, at least, as concerns carbon dioxide (the most mobile phase).

Thus, the mineral formation in veinlets was controlled by the concentrations of chemical elements in pore solution rather than by their initial distribution in particular segments of the ore layer.

ANALYSIS OF MINERAL EQUILIBRIA

The main mineral assemblages of manganese ore at the South Faizulino deposit may be characterized within the limits of the system $MnO–SiO_2–H_2O–CO_2–O_2$.

In this system, MnO and SiO_2 were accepted to be inert components, and water, carbon dioxide, and oxygen, mobile components; the number of phases (minerals) is equal to eight: quartz, pyroxmangite, neotocite, caryopilite, tephroite, ribbeite, rhodochrosite, and hausmannite; the chemical compositions of minerals are constant and do not contain such admixtures as Al, Fe, Mg, and Ca. Because thermodynamic constants for neotocite, caryopilite, and ribbeite are unknown to date, it is rational first to conduct the analysis of mineral equilibria using the method elaborated by Korzhinsky (1973) and afterwards to calculate some reactions in quantitative terms.

Plotting and analysis of a qualitative diagram. The temperature and the mole fraction of CO_2 in solution ($X_{CO_2} = n_{CO_2}/(n_{CO_2} + n_{H_2O} + n_{O_2})$) were chosen as parameters; pressure is assumed to be constant ($P_{fluid} = P_{H_2O} + P_{CO_2} + P_{O_2} = \text{const}$); oxygen concentration as a factor of equilibrium was omitted. The method of plotting of the $T–X_{CO_2}$ diagrams was considered in detail by Kerrick (1974).

Table 3. Equations of chemical reactions in the system $MnO–SiO_2–H_2O–CO_2–O_2$

No.	Equation
1	$5NeO = Car + Qtz + 2H_2O$
2	$Car + Qtz = 5Pyr + 3H_2O$
3	$Car + 3Rds = 4Teph + 3H_2O + 3CO_2$
4*	$5Car = 2Teph + 6Bem + 3H_2O$
5	$Car + 3Rib = 10Teph + 6H_2O$
6	$Pyr + CO_2 = Qtz + Rds$
7	$6Rds + O_2 = 2Hau + 6CO_2$
8	$24NeO = 2Hau = 6Car + 6H_2O + O_2$
9	$6Car + 10Hau = 12Rib + 6H_2O + 5O_2$
10	$Car = 3Pyr + Teph + 3H_2O$
11	$6Rib + O_2 = 12Teph + 2Hau + 6H_2O$
12	$4Neo + Rds = Car + H_2O + CO_2$
13	$Car + 5Rds = 2Rib + H_2O + 5CO_2$
14	$Rib + CO_2 = 2Teph + Rds + H_2O$
15	$Neo + CO_2 = Qtz + Rds + H_2O$
16	$4Qtz + 5Rds + 3H_2O = Car + 5CO_2$
17	$Car + CO_2 = 4Pyr + Rds + 3H_2O$
18	$Teph + CO_2 = Pyr + Rds$

Note: Minerals: (Qtz, 1) quartz SiO_2; (Pyr, 2) pyroxmangite $MnSiO_3$; (NeO, 3) neotocite $MnSiO_3 \cdot H_2O$; (Car, 4) caryopilite $Mn_5Si_4O_{10}(OH)_6$; (Teph, 5) tephroite Mn_2SiO_4; (Rib, 6) ribbeite $Mn_5(SiO_4)_2(OH)_2$; (Rds, 7) rhodochrosite $MnCO_3$; (Hau, 8) hausmannite $MnMn_2O_4$; (Bem) bementite $Mn_7Si_4O_{10}(OH)_{10}$. Numerals in parentheses are mineral numbers in Fig. 7. * Reaction is suggested in the studied ore but not shown in Fig. 7. Equation numbers correspond to the numbers in the text and in Fig. 7.

The diagram obtained is shown in Fig. 7a, and the respective equations of chemical reactions that proceed on lines of monovariant equilibria are listed in Table 3.

The consideration of the diagram indicates that the oxide phases (hausmannite in the modeling system) are stable only at a very low concentration of carbon dioxide (to the left of line 7). With increasing X_{CO_2}, hausmannite is replaced with rhodochrosite and with a gradual increase in temperature progressively interacts with neotocite (reaction 8), caryopilite (reaction 9), and ribbeite (reaction 11, see Table 3). As a result, oxide relics may be retained only in the areas with the lowest silica content, as has been established for hausmannite at the South Faizulino deposit, and at a minimal concentration of CO_2 in pore solution. The field of silicate stability is also located in the left part of the diagram in the region of relatively low X_{CO_2} values. To the right of lines 15, 16, and 6, silicates become unstable and are replaced by the rhodochrosite + quartz assemblage, which is retained at a high CO_2 concentration within a wide temperature range. The field of silicate stability

along the X_{CO_2} axis is wider than the field of hausmannite. Therefore, Mn silicates may coexist with both hausmannite and rhodochrosite. In the region of hausmannite stability, the formation of various silicates is controlled by temperature, and in the field of rhodochrosite stability, not only by temperature but also by the CO_2 concentration in solution.

Neotocite is the lowest temperature silicate. Caryopilite, ribbeite, tephroite, and finally pyroxmangite crystallize progressively with increasing temperature. This series is consistent with the empirically established succession of reactions in the main ore layer considered above. Caryopilite and then ribbeite break down at still higher temperatures. The fields of stability of all silicates partially overlap one another, and many possible mineral assemblages arise.

The mineral assemblages at the South Faizulino deposit cover the temperature range from reaction line 2 (the formation of pyroxmangite) to line 10 (the breakdown of caryopilite). According to geological data, this range corresponds to ~ 250°C. All minerals of the studied ore are stable under these conditions. The character of stable mineral assemblages depends on the proportion of Mn and Si, i.e., the Mn/(Mn + Si) ratio, in rock and on the mole fraction of carbon dioxide in pore solution.

In the region of minimal X_{CO_2} values (to the left of line 7), hausmannite and ribbeite coexist in high-grade Mn ore. The ribbeite + tephroite, tephroite + caryopilite, and caryopilite + pyroxmangite assemblages appear with increasing Si contents, and the ore with the lowest Mn/(Mn + Si) ratio is composed of pyroxmangite and quartz. With increasing X_{CO_2}, hausmannite is replaced by rhodochrosite and a new rhodochrosite + ribbeite assemblage arises, whereas all other assemblages remain unchanged. Further growth of the CO_2 concentration leads to the gradual reduction of a number of silicates. Ribbeite disappears first (reaction 14), and the tephroite + rhodochrosite assemblage becomes stable instead of ribbeite. Further, tephroite (reaction 3), caryopilite (reaction 17), and finally pyroxmangite (reaction 6) lose stability.

As is clearly seen from the diagram, the pyroxmangite–quartz assemblage characteristic of low-grade ore is most stable within the temperature range under consideration. This assemblage remains stable in a wide interval of X_{CO_2} and at a wide variation of the Mn/(Mn + Si) ratio in rock, from 0 to 0.5. At the same time, the mineralogy of high-grade manganese ore with Mn/(Mn + Si) = 0.5–1.0 is very sensitive to variations in rock composition and the concentration of CO_2 in solution. Even an insignificant change in any of these parameters is able to modify the phase composition of ore.

Comparison of the mineral assemblages in the modeling system with those really established in ore at the South Faizulino deposit (Figs. 2, 4a) allows the conclusion to be drawn that particular segments of the manganese layer were different not only in contents of major components but also in the CO_2 concentration in pore solution. Thus, crystallization of tephroite and ribbeite, as well as retention of hausmannite in the rock, testifies to a low CO_2 concentration. The formation of the rhodochrosite–tephroite–ribbeite–hausmannite and caryopilite–ribbeite–rhodochrosite–tephroite ores is possible only in a case where X_{CO_2} does not exceed the values constrained by reaction line 3. The occurrence of the caryopilite + rhodochrosite, pyroxmangite + rhodochrosite, and especially quartz + rhodochrosite assemblages conversely indicates that X_{CO_2} in metamorphic fluid was relatively high.

The revealed variations in the fluid composition most likely were established by a nonuniform distribution of biogenic hydrocarbons in the Mn-bearing sediments; the carbon dioxide was produced by oxidation of hydrocarbons. The higher the content of organic matter in sediment, the higher X_{CO_2} should be in the given segment of the ore layer. The CO_2 concentrations did not even out throughout the orebody, most likely, owing to the nonuniform porosity of rocks and the occurrence of poorly permeable clayey interbeds that prevented carbon dioxide from free migration.

The modeling T–X_{CO_2} diagram (Fig. 7a) clearly demonstrates the succession of mineral formation in compositionally heterogeneous manganese lodes with increasing temperature. The lower left field corresponds to the initial sedimentary ore in the chosen system, where quartz, neotocite, and hausmannite are stable. In the case of a low content of organic matter and low X_{CO_2} in pore solution, respectively, further modification of the ore mineralogy develops according to the variant designated by arrow (a) in the diagram. As a result, hausmannite-bearing ore composed of ribbeite, tephroite, caryopilite, pyroxmangite, and quartz is formed. The opposite variant, i.e., metamorphism of the sediment with a high content of organic matter, is indicated by arrow (c). According to the second scenario, hausmannite is replaced with rhodochrosite at a still low temperature and afterwards neotocite breaks down into quartz and rhodochrosite. The latter assemblage remains stable at a high temperature. Transitional variants between these extreme situations are possible; one such variants is shown by arrow (b). The combination of all variants makes up the mineralogical diversity of manganese ores.

Inasmuch as formation of many silicates was provided by decarbonation reactions, metamorphism of a manganese lode should be accompanied by removal of carbon dioxide from the system with retention of a different CO_2 concentration in various segments of the lode.

The nonuniform distribution of carbon dioxide is a main reason why the mineral assemblages of the ore

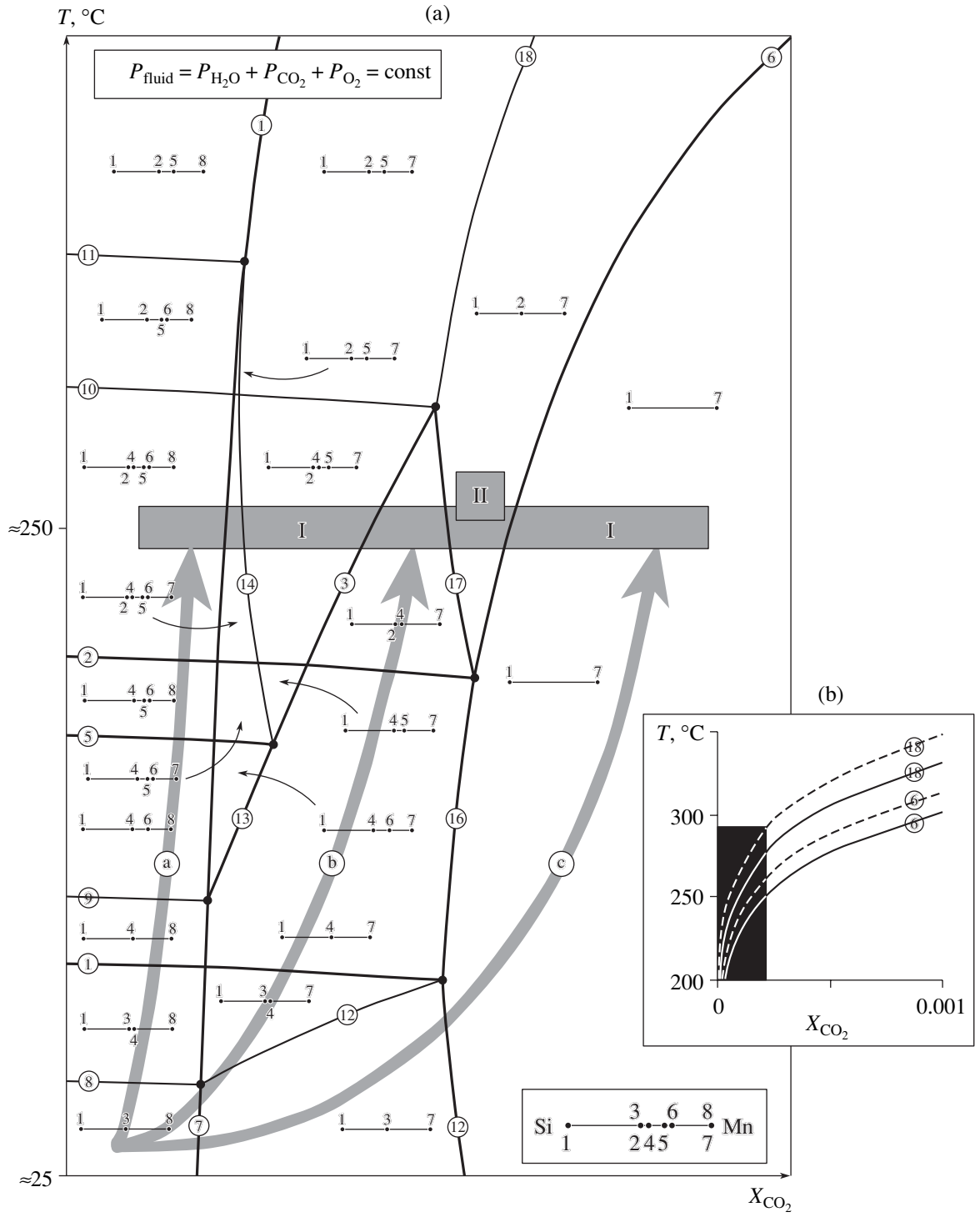

Fig. 7. (a) Mineral assemblages in the system $MnO–SiO_2–H_2O–CO_2–O_2$ depending on temperature and mole fraction of CO_2 in solution. Minerals: (1) quartz, (2) pyroxmangite, (3) neotocite, (4) caryopilite, (5) tephroite, (6) ribbeite, (7) rhodochrosite, (8) hausmannite. Numerals in circles are equation numbers in Table 3. (I) and (II) are fields of stability of mineral assemblages in (I) the main ore layer and (II) the late veinlets. Heavy lines are lines of reactions established from the observed relationships between minerals. Arrows (a–c) indicate variants of mineral formation in the rocks with variable contents of organic matter (see text for explanation). (b) Lines of equlibrium: pyroxmangite = quartz + rhodochrosite (6) and tephroite = pyroxmangite + rhodochrosite (18). Solid lines correspond to 2 kbar pressure and dashed lines, to 3 kbar. The black rectangle indicates the location of the diagram in Fig. 7a.

layer cannot be plotted on a common composition–paragenesis diagram. The second reason pertains to the relatively low-grade metamorphism of ore. As is known, the proceeding of chemical reactions at a low temperature is constrained by kinetic factors. Owing to kinetic effects, many processes remain incomplete and numerous protolith relics that make traceable the entire succession of phase transformation are left behind after virtually every reaction. The occurrence of neotocite inclusions in caryopilite aggregates, the retarded formation of pyroxmangite at the location of rhodochrosite and quartz (reaction 6), and other processes are controlled by precisely kinetic factors.

The narrow field bounded by reaction lines 6, 17, and 18 in the diagram corresponds to the mineral assemblages of the late veinlets. According to CO_2 concentrations, this field is located practically in the middle of the possible X_{CO_2} range at the deposit as a whole. Furthermore, the veinlet mineralization could have been formed at a higher temperature in comparison with the bulk of manganese ore. However, no definite geological or mineralogical evidence for a temperature rise during tectonic deformation of the ore-bearing sequence is available. Therefore, it is suggested that the concentration of carbon dioxide in solution was the main factor that regulated equilibrium in this case. In the communicating fracture network filled with pore solution, the CO_2 concentration is apparently averaged rather fast, and owing to such an averaging of fluid composition throughout the orebody, the late veinlets acquired a simple and uniform mineralic composition.

Quantitative calculations allowed the assessment of the X_{CO_2} value of metamorphism of the Mn-bearing sequence. Such calculations were performed only for two reactions: (1) interaction between rhodochrosite and quartz with formation of pyroxmangite (reaction 6) and (2) interaction between pyroxmangite and rhodochrosite with formation of tephroite (reaction 18). Despite the scantiness of these data, they nonetheless are helpful because they estimate the order of magnitude of the parameters.

The calculations were carried out making use of the internally consistent thermodynamic data set compiled by Holland and Powell (1990, 1998) and following a well-known technique (Zharikov, 1976; Bulakh and Krivovichev, 1985; Berman, 1991). The calculation results are presented in Fig. 7b. Comparison of these results with the qualitative T–X_{CO_2} diagram considered above shows that, at a temperature of 250°C and a pressure of 2 kbar, the fields of stability of most mineral assemblages in the manganese ore at the South Faizulino deposit correspond to X_{CO_2} values less than 0.00025. An increase in pressure to 3 kbar narrows this space by almost two times.

Thus, at low temperatures, Mn silicates are formed at very low concentrations of CO_2 in solution and extremely insignificant fluctuations of X_{CO_2} may change the composition of mineral assemblages.

CONCLUSIONS

(1) Thirty-two minerals have been identified in the main ore layer and in the late veinlets at the South Faizulino deposit. Quartz, hausmannite, rhodochrosite, tephroite, ribbeite, pyroxmangite, and caryopilite are the major minerals.

(2) The minerals in the main ore layer were formed in the course of burial metamorphism at a maximum temperature and pressure of 250°C and 2.5 kbar, respectively.

(3) The initial sediments were heterogeneous in contents of Mn, SiO_2, organic matter, and other components. Manganese accumulated largely in the oxide form and as a Mn–Si gel-like phase. In the process of diagenesis, oxidation of biogenic hydrocarbons and a related increase in CO_2 concentration in solution resulted in replacement of most of the oxides with rhodochrosite, whereas the Mn–Si gel was transformed into neotocite and partly replaced with carbonate.

(4) A gradual increase in temperature and pressure led to the replacement of neotocite with caryopilite, which further participated in reactions that gave rise to the formation of ribbeite, tephroite, pyroxmangite, and other minerals. Hence, crystallization of many silicates resulted from transformation of the initial Mn–Si gel.

(5) Caryopilite with insignificant Al, Fe, and Mg contents is stable only at a low temperature (<300°C). The occurrence of these admixtures in significant amounts widens the temperature range of caryopilite stability.

(6) The formation of pyroxmangite and rhodonite depended on the Ca distribution in ore at constant temperature and pressure. Pyroxmangite was formed in ore depleted in Ca, whereas enrichment in Ca led to the appearance of rhodonite.

(7) Crystallization of spessartine in Mn ore does not require such high temperatures as follow from experimental results (Hsu, 1968).

(8) In addition to *PT* parameters, the formation of various assemblages of metamorphic minerals was controlled by the Mn/(Mn + Si) ratio in ore and X_{CO_2} in pore solution. In high-grade Mn ore, low CO_2 concentrations stabilized hausmannite, ribbeite, tephroite, and caryopilite. The pyroxmangite–rhodochrosite and quartz–rhodochrosite assemblages were formed at the same Mn and Si contents but at higher X_{CO_2} values. The variable concentrations of carbon dioxide in solution were probably caused by different contents of organic matter in the initial sediments and by sluggish diffusion of components between different segments of the ore layer.

(9) At a low temperature, the formation of Mn silicates is possible only at low CO_2 concentrations in solution ($X_{CO_2} < 0.00025$). Even insignificant fluctuations of X_{CO_2} may change the composition of mineral assemblages drastically. An increase in pressure narrows the field of silicate stability still more.

(10) In the process of hydrothermal metasomatic mineral formation in veinlets, the substance migrated for a very short distance that was not greater than the thickness of the Mn-bearing layer. The major components of ore (Mn, Si, and CO_2) were mainly involved in redistribution. The infiltration of solutions through a network of communicating fractures led to the rapid averaging of their composition. As a result, the late veinlets are similar in composition throughout the deposit.

ACKNOWLEDGMENTS

This work was supported by the Russian Foundation for Basic Research, project no. 04-05-64333.

REFERENCES

1. B. Aleksiev, "Neotocite from the Oligocene Manganese Ore Unit in the Varna Region," Mineral. Sb. L'vov. Geol. O–va, No. 14, 208–214 (1960).
2. P. F. Andrushchenko, A. T. Suslov, and N. V. Gavashvili, "Manganese Deposits in the Tetritskaroi Ore District, Georgia," in *Volcanosedimentary and Hydrothermal Manganese Deposits (Central Kazakhstan, Lesser Caucasus, Yenisei Range)* (Nauka, Moscow, 1985), pp. 115–172 [in Russian].
3. R. G. Berman, "Thermobarometry Used Multiequilibrium Calculations: A New Technique with Petrological Application," Can. Mineral. **29**, 833–855 (1991).
4. A. I. Brusnitsyn and N. V. Chukanov, "Ribbeite and Alleghanyite from Manganese Rocks in the South Faizulino Deposit (Southern Urals)," Zap. Vseross. Mineral. O–va **131** (5), 98–111 (2002).
5. A. I. Brusnitsyn and I. G. Zhukov, "South Faizulino Manganese Deposit (Southern Urals, Russia): Geology, Petrography, and Formation Processes," Litol. Polezn. Iskop. **40** (1), 35–55 (2005) [Lithol. Miner. Res. **40** (1), (2005)].
6. A. G. Bulakh and V. G. Krivovichev, *Calculation of Mineral Equilibria* (Nedra, Leningrad, 1985) [in Russian].
7. A. M. Clark, A. J. Easton, and G. C. Jones, "A Study of the Neotocite Group," Mineral. Mag. **42**, M26–M30 (1978).
8. *Copper Massive Sulfide Deposits in the Urals: Geological Factors of Localization*, Ed. by V. I. Smirnov (Ural. Sci. Center, Acad. Sci. USSR, Sverdlovsk, 1985) [in Russian].
9. N. L. Dobretsov, "Relationships between Tectonics and Metamorphism," Petrologiya **3** (1), 4–23 (1995).
10. R. L. Dobretsov, V. S. Sobolev, and V. V. Khlestov, *Facies of Regional Metamorphism of Moderate Pressure* (Nedra, Moscow, 1972) [in Russian].
11. R. A. Eggleton, J. H. Pennington, R. S. Freeman, et al., "Structural Aspect of the Hisingerite–Neotocite Series," Clay Mineral. **18** (1), 21–31 (1983).
12. M. J. K. Flohr and J. S. Huebner, "Mineralogy and Geochemistry of Two Metamorphosed Sedimentary Manganese Deposits, Sierra Nevada, California, USA," Lithos **29**, 57–85 (1992).
13. A. A. Gavrilov, *Exhalation–Sedimentary Ore Deposition (with Reference to the Urals and Kazakhstan)* (Nedra, Moscow, 1972) [in Russian].
14. S. Guggenheim and R. A. Eggleton, "Crystal Chemisrty, Classification, and Identification of Modulated Layer Silicates," Rev. Mineral. **19**, 665–725 (1988).
15. S. Guggenheim and R. A. Eggleton, "Modulated Crystal Structures of Greenalite and Caryopilite: A System with Long-Range, In-Plane Structural Disorder in the Tetrahedra Sheet," Can. Mineral. **36**, 163–179 (1998).
16. M. H. Hey, "A New Review of the Chlorites," Mineral. Mag. **30**, 1–277 (1954).
17. T. J. B. Holland and R. Powell, "An Enraged and Undated Internally Consistent Thermodynamic Data Set with Uncertainties and Correlation: the System K_2O–Na_2O–CaO–MgO–FeO–Fe_2O_3–Al_2O_3–TiO_2–SiO_2–C–H_2–O_2," J. Metamorph. Geol **89**, 1404–1414 (1990).
18. T. J. B. Holland and R. Powell, "An Internally Consistent Thermodynamic Data Set for Phases of Petrological Interest," J. Metamorph. Geol. **16**, 309–343 (1998).
19. L. S. Hsu, "Selected Phase Relationships in the System Al–Mn–Fe–Si–O–H: A Model for Garnet Equilibrium," J. Petrol. **9**, 40–83 (1968).
20. J. S. Huebner, M. J. K. Flohr, and J. N. Grossman, "Chemical Fluxes and Origin of Manganese Carbonate–Oxide–Silicate Deposits in Bedded Chert," Chem. Geol. **100**, 93–118 (1992).
21. V. V. Kalinin, "Manganese and Ferromanganese Deposits on the Eastern Slope of the Southern Urals," in *Manganese Deposits in Foldbelts of the USSR* (Nauka, Moscow, 1978), pp. 55–90 [in Russian].
22. D. M. Kerrick, "Review of Metamorphic Mixed-Volatile (H_2O–CO_2) Equilibrium," Am. Mineral. **59**, 729–762 (1974).
23. E. S. Kontar, K. P. Savel'eva, A. V. Surganov, et al., *Manganese Deposits of the Urals* (Ural Geological Mapping Expedition, Yekaterinburg, 1999) [in Russian].
24. D. S. Korzhinsky, *Theoretical Principles of the Analysis of Mineral Parageneses* (Nauka, Moscow, 1973) [in Russian].
25. N. I. Krasnova and T. G. Petrov, "Genesis of Mineral Individuals and Aggregates," (Nevskii Kur'er, St. Petersburg, 1997) [in Russian].
26. V. N. Kuleshov and A. I. Brusnitsyn, "A New Mechanism of Formation of Carbonate Manganese Ore from $\delta^{13}C$ and $\delta^{18}O$ for the South Faizulino Deposit, Southern Urals)," Dokl. Akad. Nauk **395** (5), 661–666 (2004) [Dokl. Earth Sci. **395A** (3), 411–415 (2004)].
27. J. G. Liou, S. Maruyama, and M. Cho, "Phase Equilibria and Mineral Parageneses of Metabasites in Low-Grade Metamorphism," Mineral. Mag. **49**, 321–333 (1985).
28. N. V. Logvinenko and L. V. Orlova, *Formation and Alteration of Sedimentary Rocks on Continent and in Ocean* (Nedra, Leningrad, 1987) [in Russian].

29. B. M. Mikhailov, "Topical Problems of Forecasting of Manganese Deposits in the Urals," Litol. Polezn. Iskop. **36** (1), 3–15 (2001) [Lithol. Miner. Res. **36** (1), 1–12 (2001)].
30. *Minerals. Reference Book*, Ed. by N. N. Smol'yaninova (Nauka, Moscow, 1992), Vol. IV (2) [in Russian].
31. F. K. Nyame, "Petrological Significance of Manganese Carbonate Inclusions in Spessartine Garnet and Relation to the Stability of Spessartine in Metamorphosed Manganese-Rich Rocks," Contrib. Mineral. Petrol. **141**, 733–746 (2001).
32. S. Roy, *Manganese Deposits* (Academic Press, London, 1981; Mir, Moscow, 1986)
33. V. L. Rusinov, V. P. Loginov, and P. I. Pirozhok, "Paragenetic Analysis of Wall-Rock Metasomatites," in *Copper Massive Sulfide Deposits of the Urals*, Ed. by S. N. Ivanov and V. A. Prokina (Ural. Division, Russ. Acad. Sci., Yekaterinburg, 1992) [in Russian].
34. I. B. Seravkin, A. M. Kosarev, D. N. Salikhov, et al., *Volcanism in the Southern Urals* (Nauka, Moscow, 1992) [in Russian].
35. H. Strunz and E. H. Nickel, *Strunz Mineralogical Tables* (Schweirerbart, Stuttgart, 2001).
36. T. Theye, W. Schreyer, and A. M. Fransolet, "Low-Temperature, Low-Pressure Metamorphism of Mn-Rich Rocks in the Lienne Syncline, Venn-Stavelot Massif (Belgian Ardennes), and the Role of Carpholite," J. Petrol. **37** (5), 767–783 (1996).
37. V. V. Zaikov, *Volcanism and Sulfide Mounds at Paleooceanic Margins (with Reference to Massive Sulfide Ore Zones in the Urals and Siberia)* (Nauka, Moscow, 1991) [in Russian].
38. E. V. Zaikova and V. V. Zaikov, "Evidence for Near-Bottom Hydrothermal Origin of Cherty Iron Edifices in the Magnitogorsk–Mugodzhary Island-Arc System of the Urals," in *Metallogeny of Ancient and Modern Oceans, 2003. Origin and Exploration of Ore Deposits in Island-Arc Systems* (Inst. Mineral., Miass, 2003), pp. 208–215 [in Russian].
39. V. A. Zharikov, *Principles of Physicochemical Petrology* (Moscow State Univ., Moscow, 1976) [in Russian].